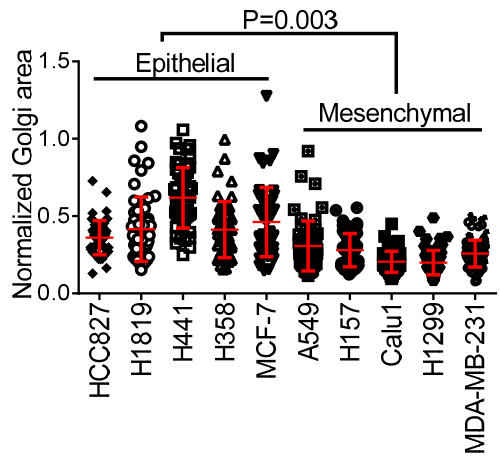
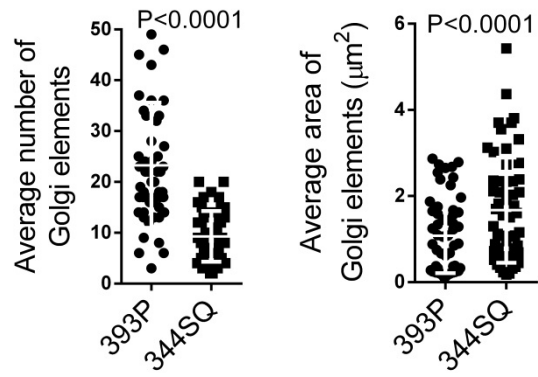


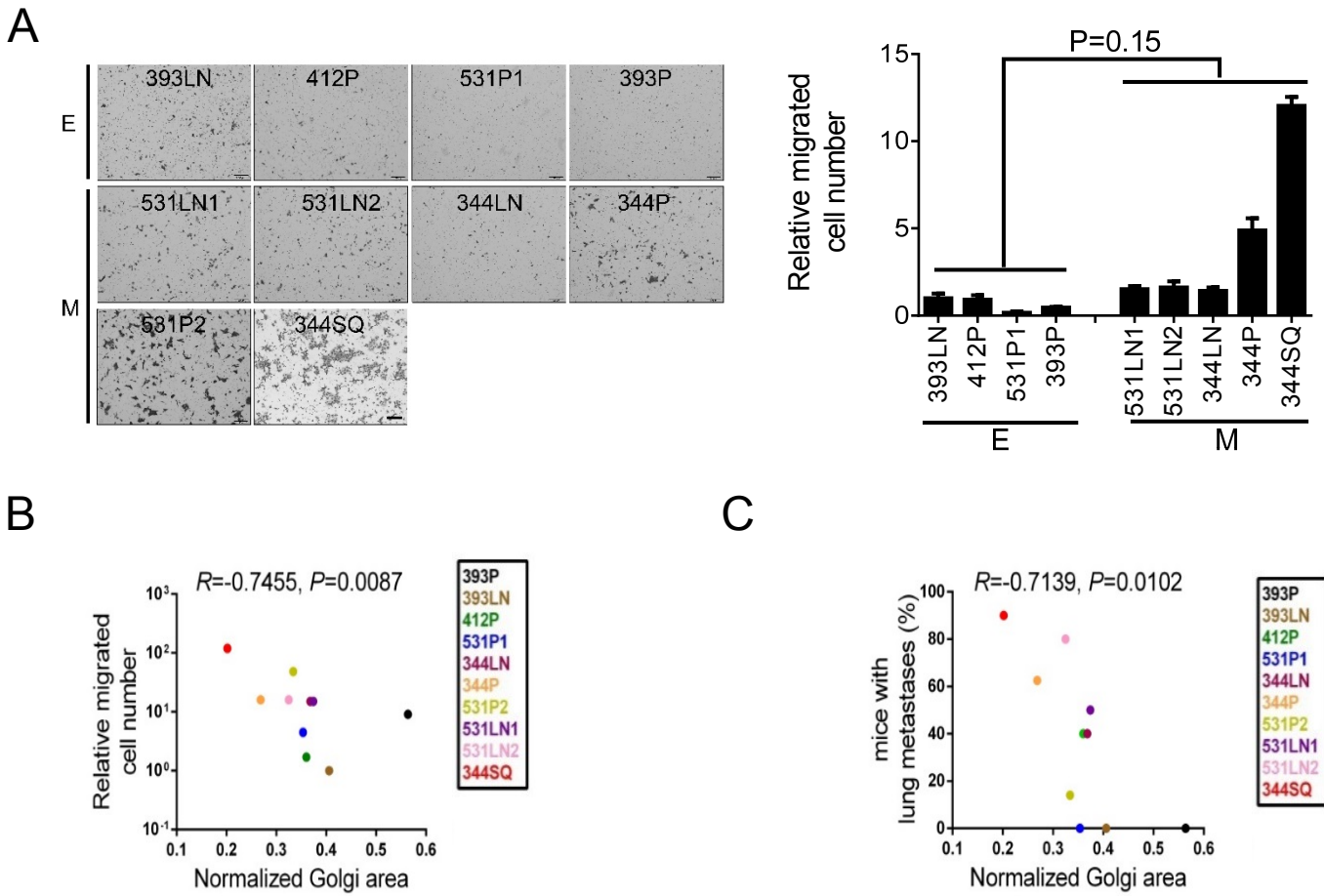
A



B

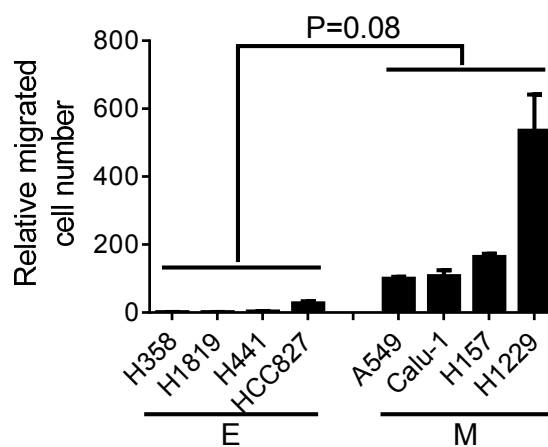
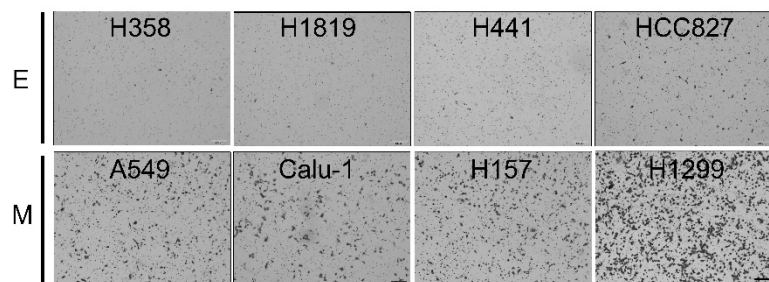


**Supplemental Figure 1. Golgi compaction and Golgi element condensation in mesenchymal tumor cells.** (A) The scatter plot shows Golgi areas normalized to nuclear areas in epithelial and mesenchymal human lung and breast (MDA-MB-231) cancer cell lines. Each dot represents values from a single cell. (B) Scatter plots show the average Golgi element numbers (left) and areas (right) in epithelial 393P cells and mesenchymal 344SQ cells. Each dot represents values from a single cell. P values determined using two-tailed Student's t-test. Results from single experiments were replicated ( $n \geq 2$  experiments).

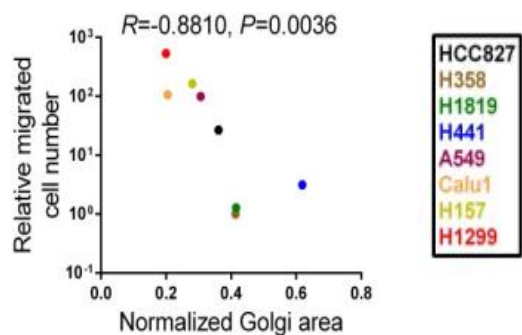


**Supplemental Figure 2. Golgi compaction is correlated with increased migratory and metastatic properties in KP cells.** (A) Bright field micrographs of migrated KP cells in Boyden chambers. Migrated cells were stained with crystal violet. Scale bars, 200  $\mu$ m. Bar graph to the right of the images shows the quantification of migrated epithelial (E) and mesenchymal (M) KP cells ( $n=3$  samples per cell line). P values determined using two-tailed Student's t-test. (B) Scatter plots show the mean Golgi areas in KP cell lines relative to the mean number of migrated cells in Boyden chambers. Golgi areas determined from at least 50 cells per cell line. (C) Scatter plot shows the mean Golgi areas in KP cell lines relative to the percentages of flank tumor-bearing mice with detectable lung metastases 3 weeks following injection of KP cells. Golgi areas determined from at least 50 cells per cell line.  $R$  and  $P$ , 2-tailed Pearson's  $r$  correlation test. Results from single experiments were replicated ( $n \geq 2$  experiments).

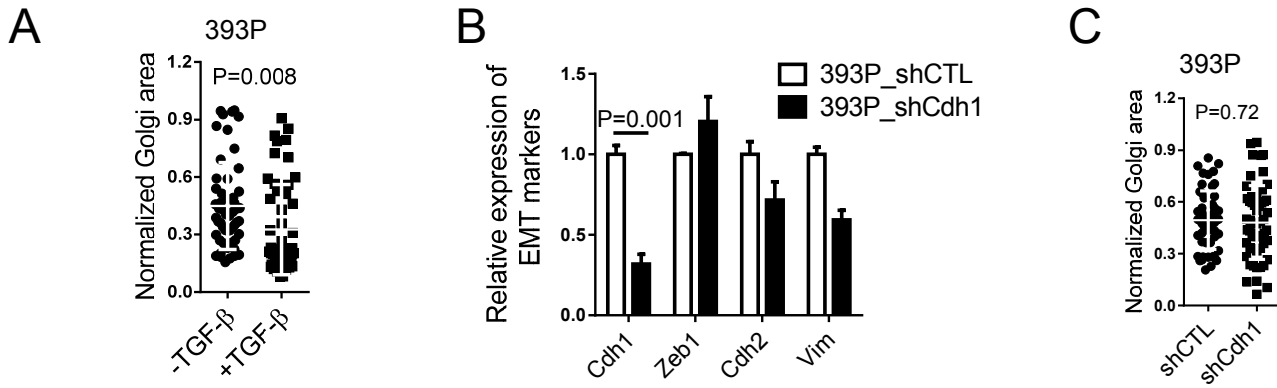
A



B

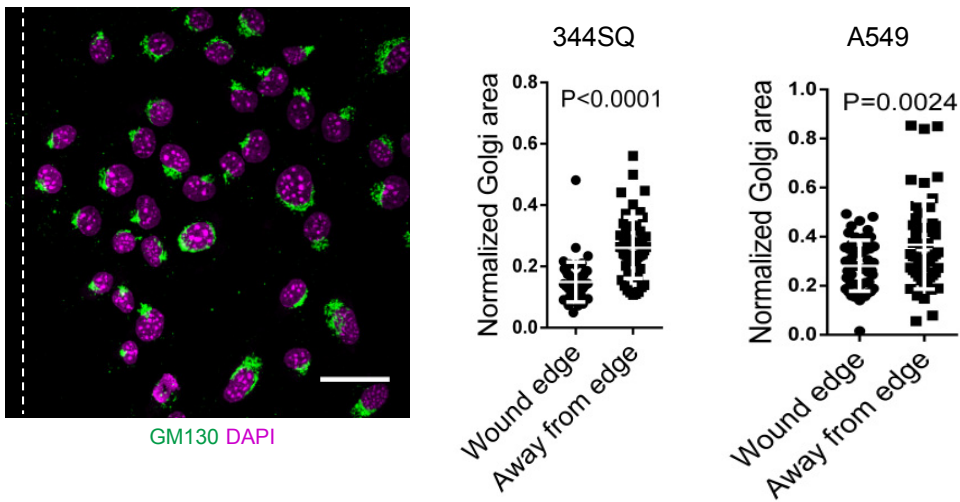


**Supplemental Figure 3. Golgi compaction in human lung adenocarcinoma cells is correlated with increased migratory properties.** (A) Bright field micrographs of migrated human lung cancer cells in Boyden chambers. Migrated cells were stained with crystal violet. Scale bars, 200  $\mu$ m. Bar graph to the right of the images shows the quantification of migrated epithelial (E) and mesenchymal (M) human lung cancer cells ( $n=3$  samples per cell line). P values determined using two-tailed Student's t-test. (B) Scatter plots show the mean Golgi areas in human lung cancer cell lines relative to the mean number of migrated cells in Boyden chambers. Golgi areas determined from at least 50 cells per cell line.  $R$  and  $P$ , 2-tailed Pearson's  $r$  correlation test. Results from single experiments were replicated ( $n \geq 2$  experiments).

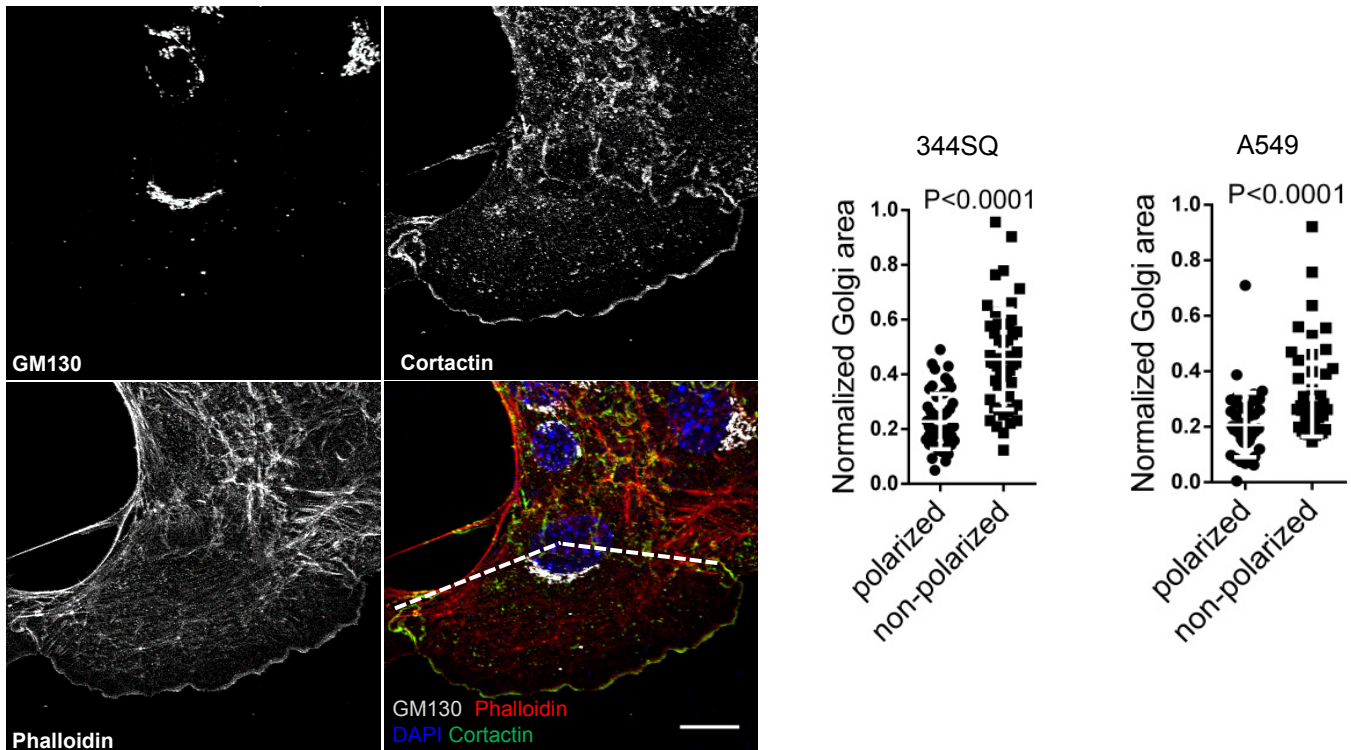


**Supplemental Figure 4. Golgi compaction is enhanced by TGF $\beta$  treatment but not E-cadherin depletion.** (A) Scatter plot shows normalized Golgi areas in 393P cells treated for 3 days with or without TGF- $\beta$  (5ng/mL). Each dot represents values from a single cell. (B) The bar graph shows the results of qPCR analysis of mRNA levels of epithelial (CDH1) and mesenchymal (Vim, Cdh2, Zeb1) markers in 393P cells stably transfected with scrambled control shRNA (shCTL) or Cdh1 shRNA (shCdh1) (n=3 samples per condition). (C) Scatter plot shows normalized Golgi areas in 393P cells stably transfected with shRNAs against E-cadherin (shCdh1) or scrambled shRNA (shCTL). Each dot represents values from a single cell. P values determined using two-tailed Student's t-test. Results from single experiments were replicated (n  $\geq$  2 experiments).

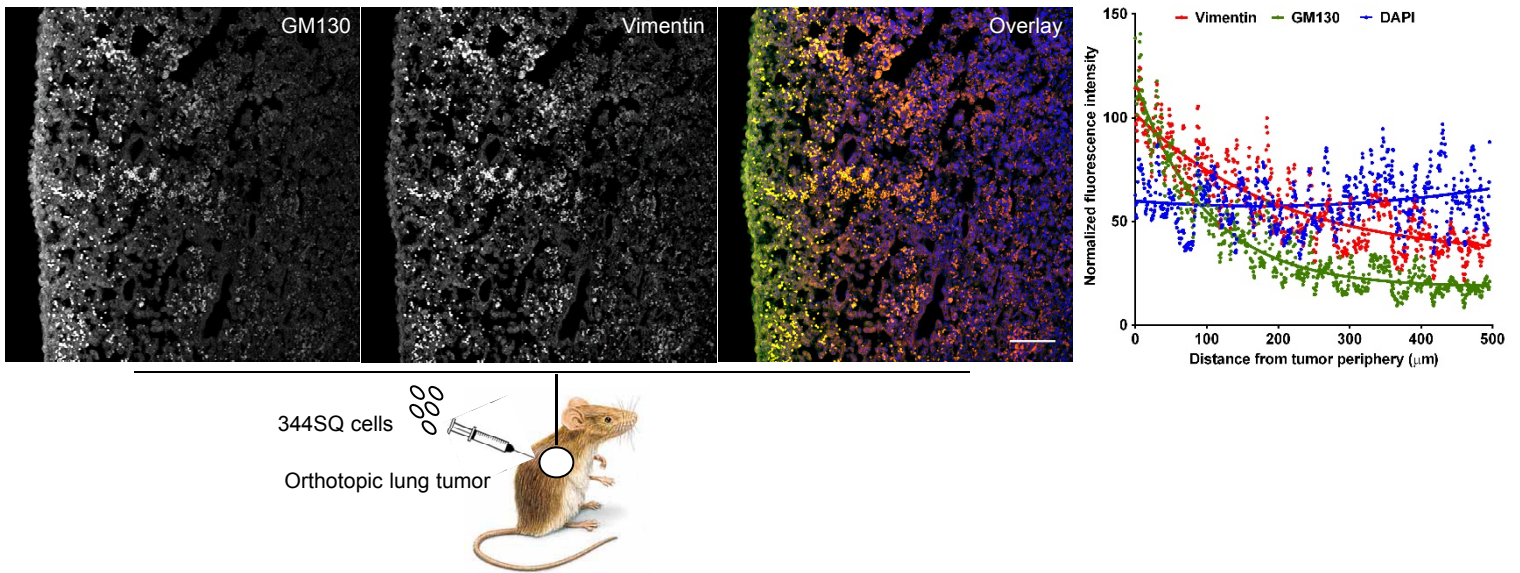
A



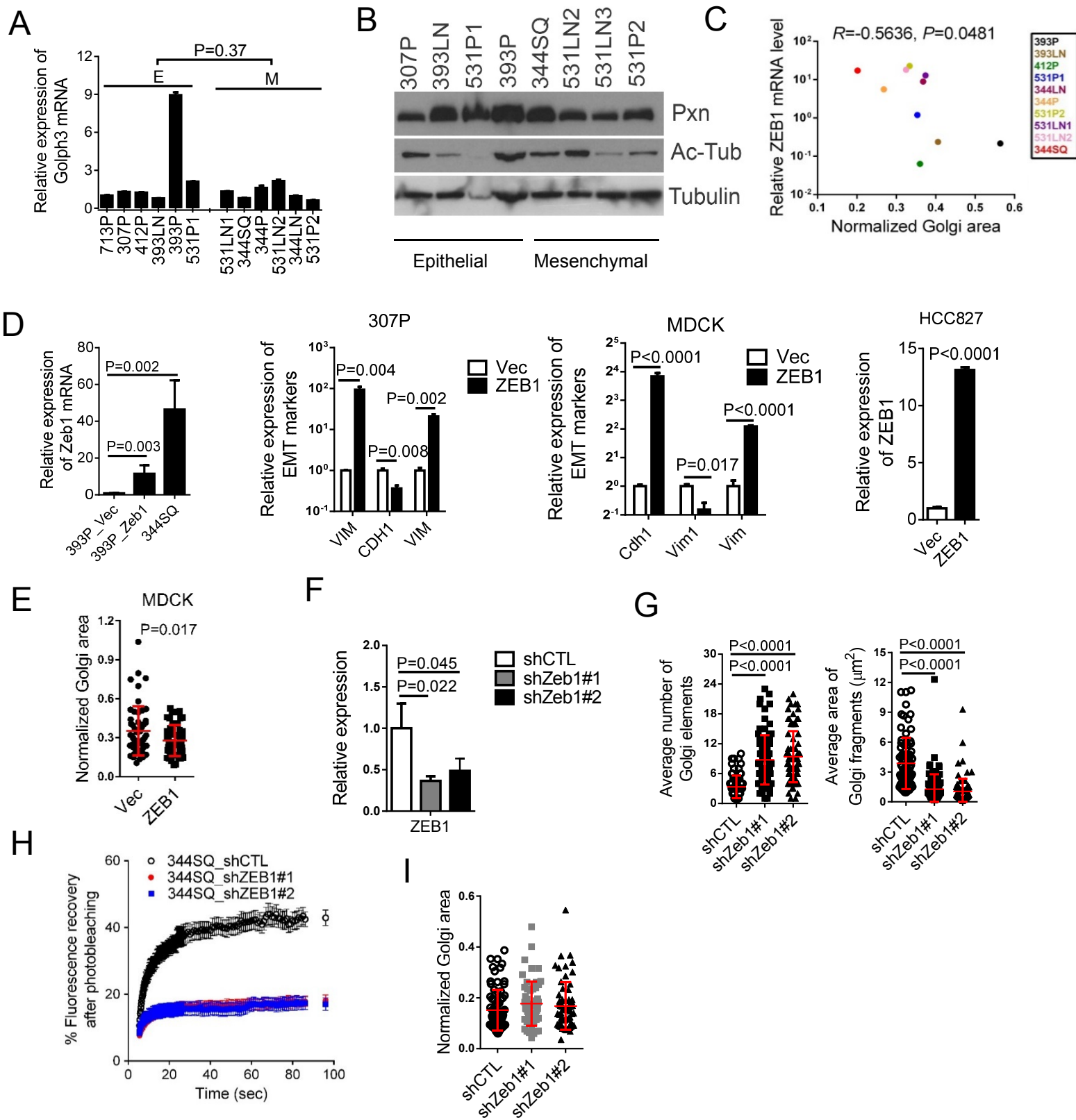
B



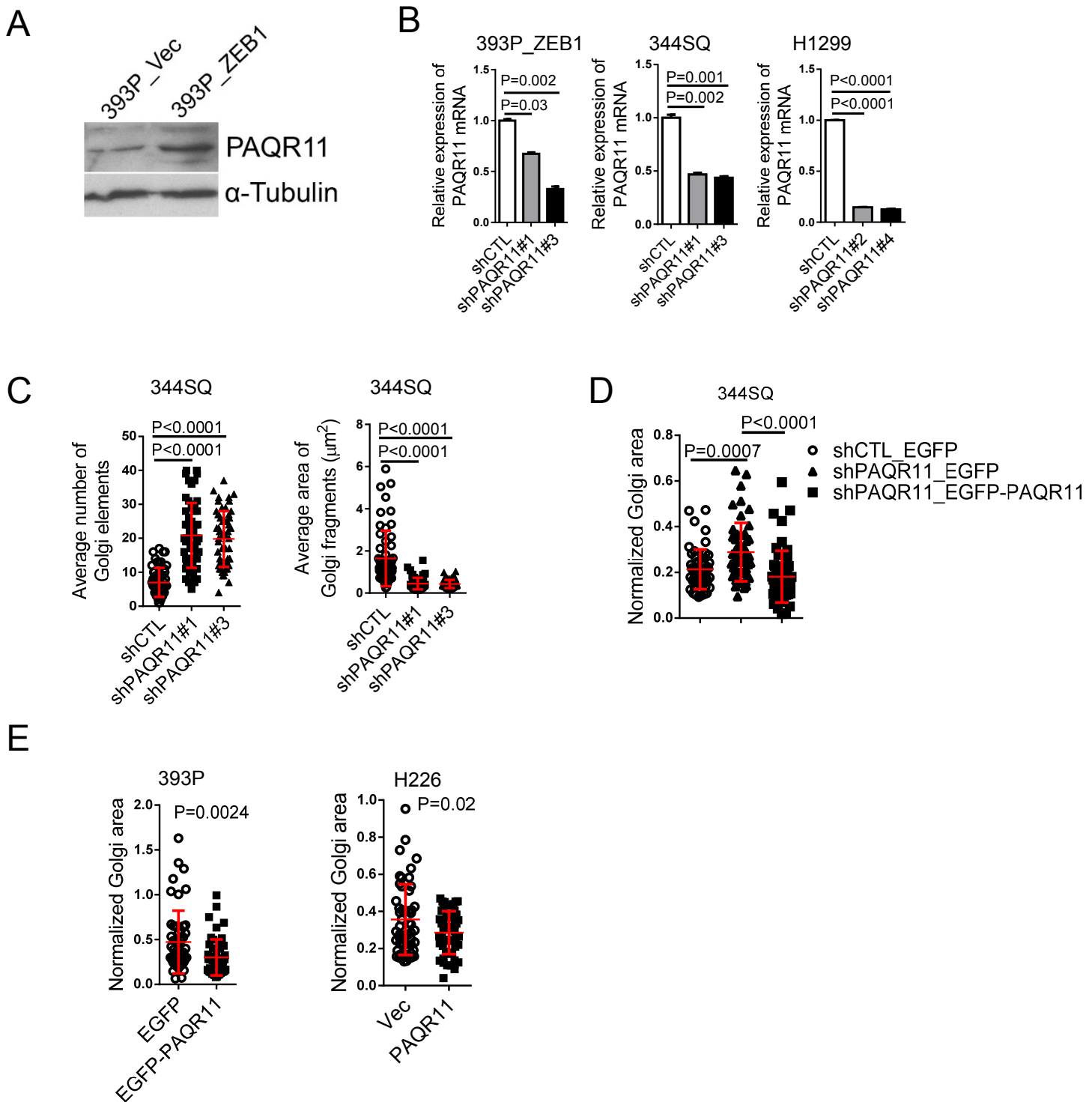
**Supplemental Figure 5. Golgi compaction occurs in cells at the leading edge of a healing wound.** (A) Confocal micrograph of Golgi (GM130, green) and nuclei (DAPI, magenta) in 344SQ cells at the leading edge of a scratch wound (wound edge indicated by vertical dotted line on left). Scale bar, 30 μm. The scatter plots show normalized Golgi areas in 344SQ cells (left) and A549 cells (right). "Wound edge" was defined as those cells on the forefront of the wound edge. Cells "away from the wound edge" were located multiple cells away from the edge in the interior of the scratch cultures. (B) Confocal micrographs of a 344SQ cell at the wound edge stained with phalloidin and antibodies against GM130 or cortactin. In the merged image (bottom right), the Golgi is confined within an area whose boundaries are indicated by dotted lines connecting the center of the nucleus (DAPI, blue) to the edges of the lamellipodium (subcortical cortactin, green). Scale bar, 15 μm. Scatter plots to the right of the micrographs show normalized Golgi areas in 344SQ cells (left) and A549 cells (right) at the wound edge scored as having polarized Golgi (confined within the area delineated above) or non-polarized Golgi (partially or totally outside of the area delineated above). P values determined using two-tailed Student's t-test. Results from single experiments were replicated ( $n \geq 2$  experiments).



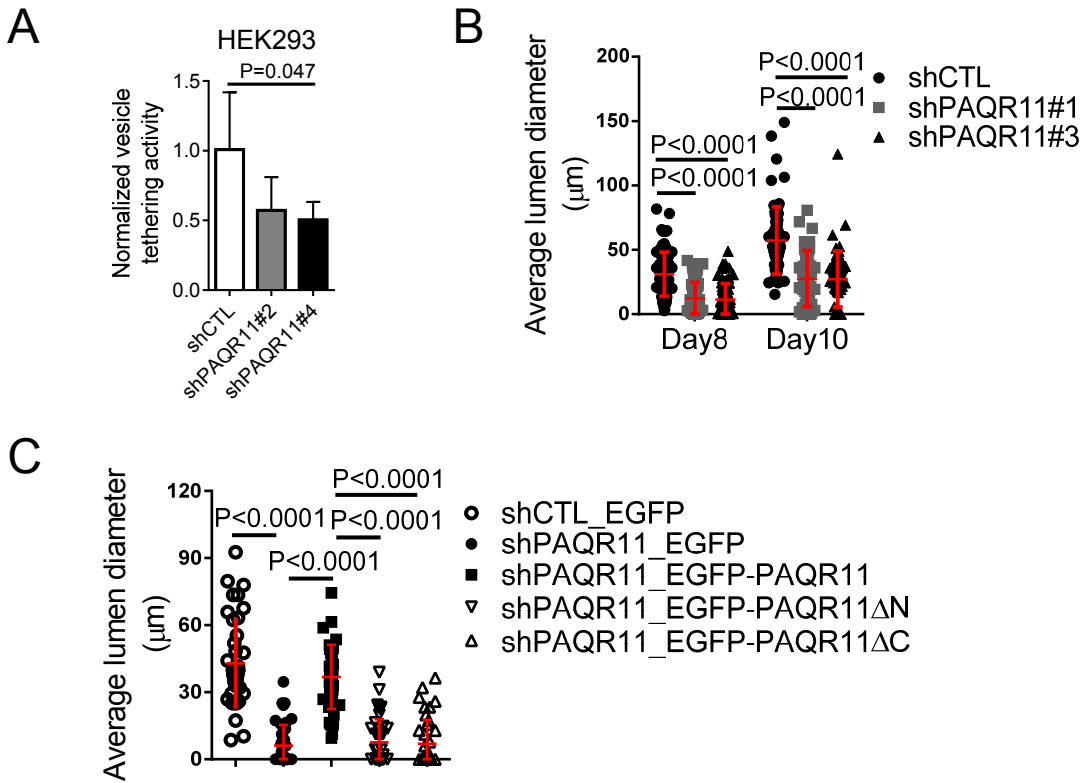
**Supplemental Figure 6. EMT leads to increased Golgi compaction.** Confocal micrographs of an orthotopic lung tumor formed by intrathoracic injection of 344SQ cells into a syngeneic, immunocompetent mouse. Nuclei were counterstained with DAPI (blue) and merged with GM130 (green) and vimentin (red) in an overlaid image (right). Scale bars, 75  $\mu\text{m}$ . The scatter plot shows normalized fluorescence intensities of cells (dots) measured radially inwards from the tumor periphery. The curve fits for vimentin, GM130, and DAPI (red, green, and blue lines, respectively) were obtained from non-linear regression using a 1-phase exponential decay equation. Results are a composite of values from orthotopic lung tumors generated in 3 mice.



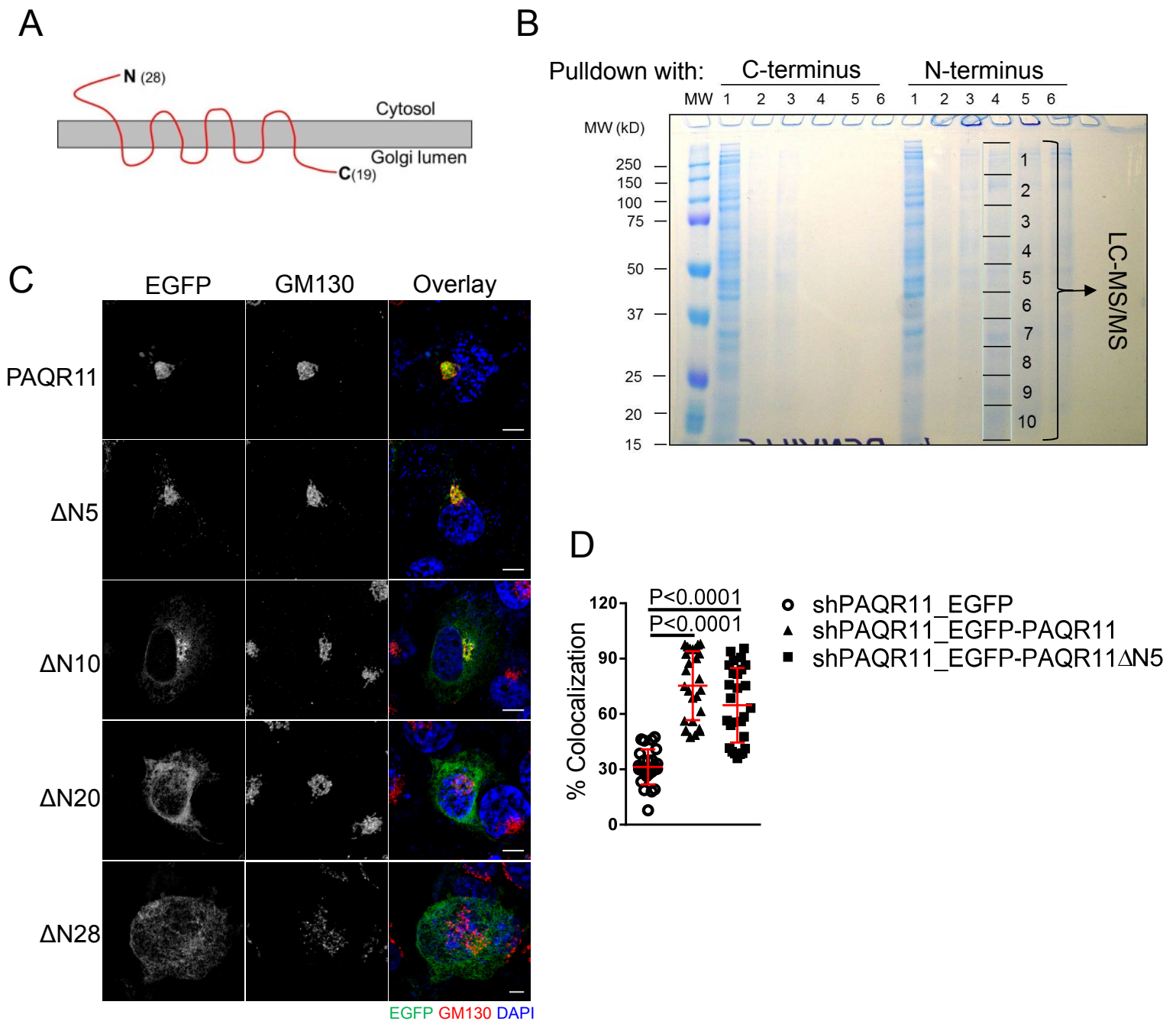
**Supplemental Figure 7. Golgi compaction is regulated by ZEB1.** (A) qPCR analysis of GOLPH3 mRNA levels in epithelial (E) and mesenchymal (M) KP cell lines. (B) Western blot analysis of paxillin (Pxn) and acetylated  $\alpha$ -tubulin (Ac-Tub) in KP cells. (C) Scatter plot shows mean Golgi areas in KP cell lines relative to endogenous ZEB1 mRNA levels ( $n > 20$  cells per cell line).  $R$  and  $P$ , 2-tailed Pearson's  $r$  correlation test. (D) The bar graphs show qPCR analysis of mRNA levels in 393P cells, 307P cells, HCC827 cells, and Madin Darby canine kidney (MDCK) cells stably transfected with empty (vec) or ZEB1 expression vector. Ectopic ZEB1 levels in 393P\_ZEB1 cells are less than endogenous ZEB1 levels in 344SQ cells (far left bar graph). Ectopic ZEB1 expression induced gene expression changes consistent with EMT. (E) Scatter plot shows Golgi areas normalized to nuclear areas in MDCK cells (dots) stably transfected with empty (Vec) or ZEB1 expression vectors. (F) Bar graph shows qPCR analysis of ZEB1 levels in 344SQ cells stably transfected with ZEB1 shRNAs (#1 or #2) or scrambled control shRNA (shCTL). Results are expressed as a ratio (shZEB1/shCTL), with 344SQ\_shCTL set at 1.0. (G) Scatter plots show the average Golgi element numbers (left) and areas (right) in 344SQ cells stably transfected with scrambled shRNA (shCTL) or ZEB1 shRNAs. Each dot represents values from a single cell. (H) Scatter plot shows the intensity recovery profile (%) of EGFP-tagged GalNAcT after photobleaching ( $n \geq 25$  cells per group). (I) Scatter plot shows the normalized Golgi areas in 344SQ cells (dots) stably transfected with scrambled shRNA (shCTL) or ZEB1 shRNAs. For bar graphs, results represent the averages of triplicate samples per condition. Unless otherwise indicated,  $P$  values from two-tailed Student's  $t$ -test or ANOVA for comparisons between 2 groups or more than 2 groups, respectively. Results from single experiments were replicated ( $n \geq 2$  experiments). See complete unedited blots in the supplemental material



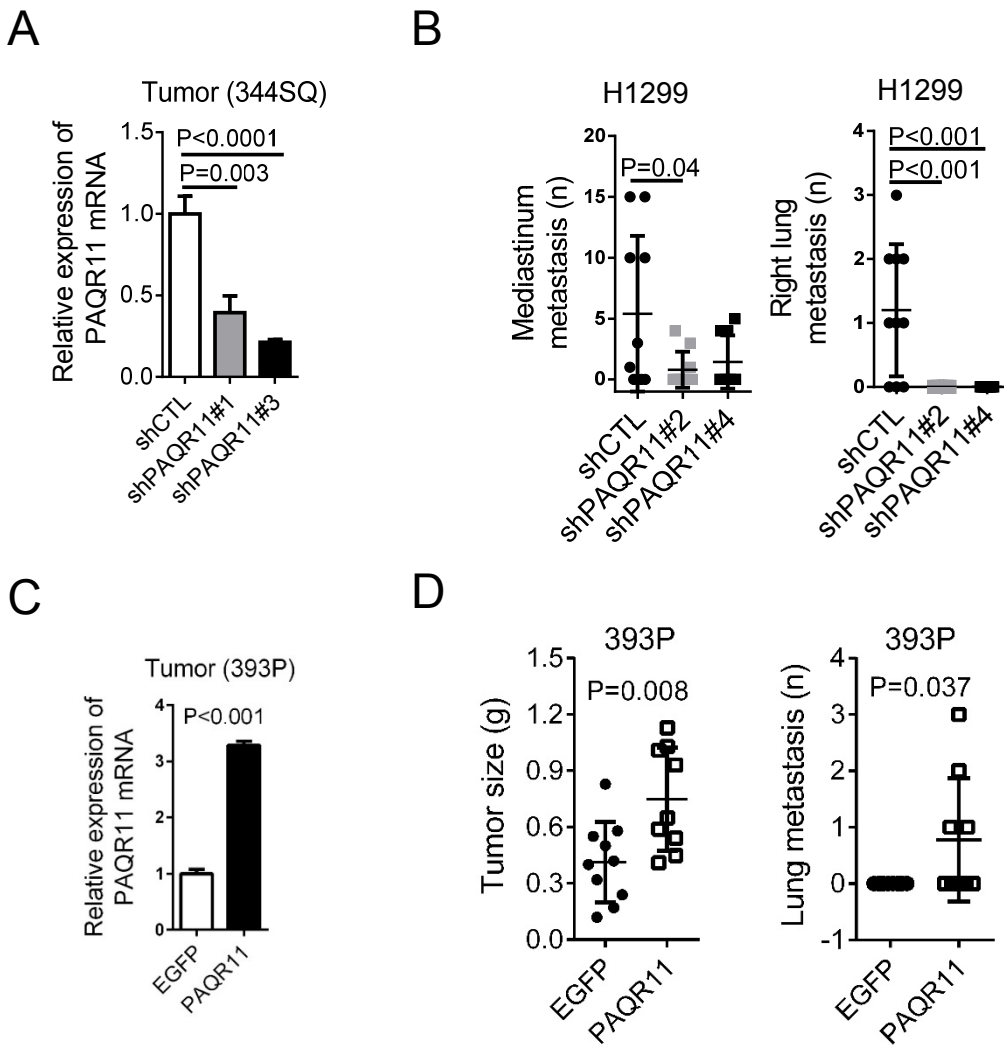
**Supplemental Figure 8. PAQR11 enables Golgi compaction.** (A) Western blot analysis of PAQR11 levels in 393P cells stably transfected with empty (Vec) or ZEB1 expression vectors.  $\alpha$ -tubulin was included as loading control. (B) The bar graphs show the results of qPCR analysis of PAQR11 mRNA levels in 393P\_ZEB1 cells (left), 344SQ cells (middle), and H1299 cells (right) stably transfected with different PAQR11 shRNAs (shPAQR11) or scrambled control shRNA (shCTL) expressed as a ratio (shPAQR11/shCTL). The levels in shCTL-transfected cells were set at 1.0 (n=3 samples per condition). (C) Scatter plots show the average Golgi element numbers (left) and areas (right) in 344SQ cells stably transfected with scrambled control shRNA (shCTL) or one of two distinct PAQR11 shRNAs (shPAQR11#1 or shPAQR11#3) (dots). Each dot represents values from a single cell. (D) The scatter plot shows Golgi areas normalized to nuclear areas in 344SQ\_shCTL cells stably transfected with EGFP (shCTL\_EGFP), 344SQ\_shPAQR11 cells stably transfected with EGFP (shPAQR11\_EGFP), and 344SQ\_shPAQR11 cells stably transfected with PAQR11 expression vector (shPAQR11\_EGFP-PAQR11). Each dot represents values from a single cell. (E) The scatter plot shows Golgi areas normalized to nuclear areas in 393P cells and H226 cells stably transfected with vectors that express nothing (Vec), EGFP alone (EGFP), PAQR11, or EGFP-tagged PAQR11 (EGFP-PAQR11). Each dot represents values from a single cell. P values from two-tailed Student's t-test or ANOVA for comparisons between 2 groups or more than 2 groups, respectively. Results from single experiments were replicated (n  $\geq$  2 experiments). See complete unedited blots in the supplemental material.



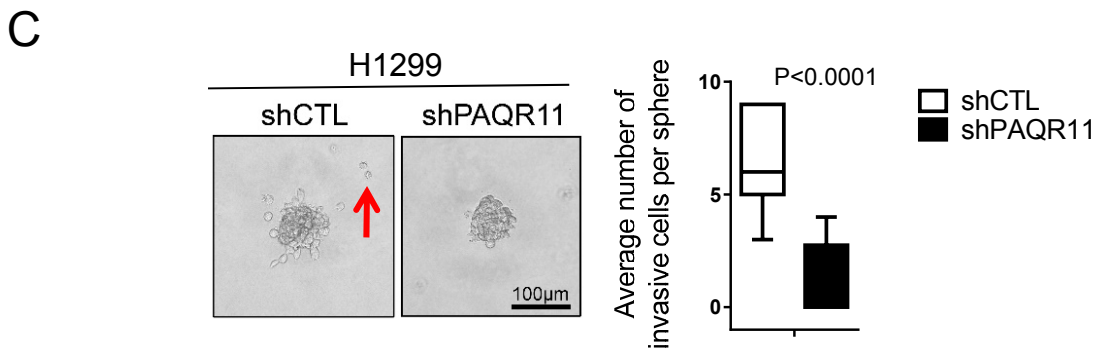
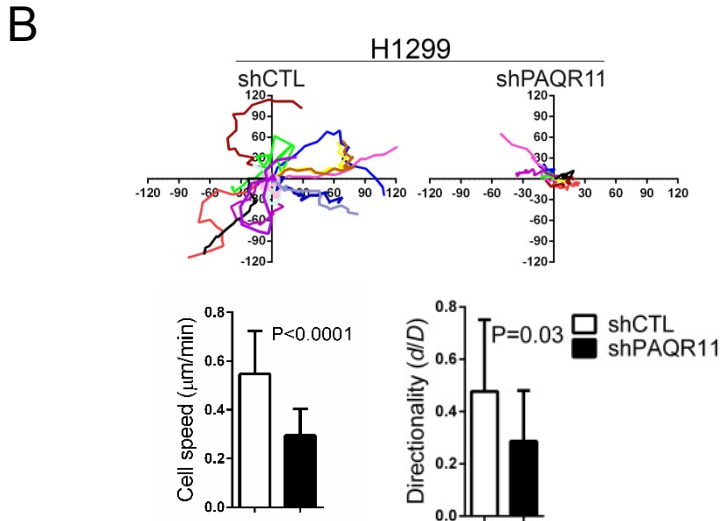
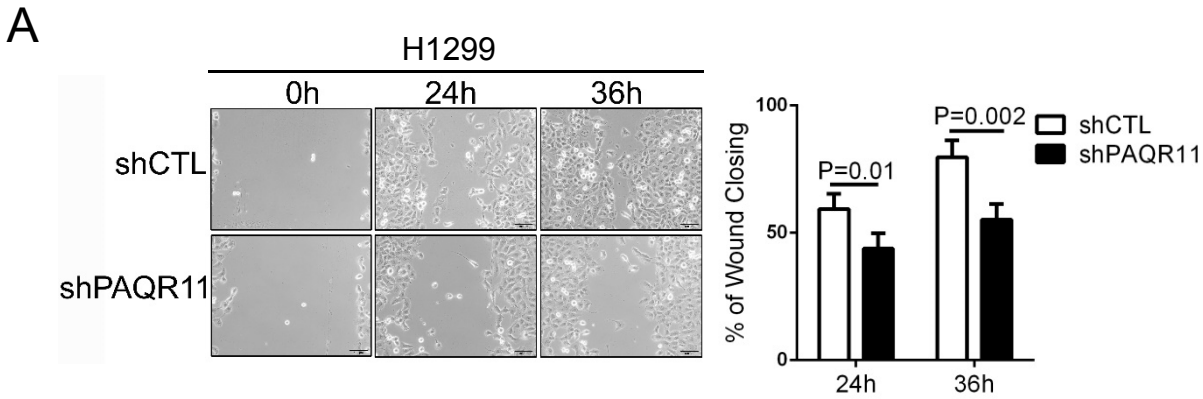
**Supplemental Figure 9. PAQR11 depletion impairs retrograde vesicle tethering to Golgi and lumen formation in spheres.** (A) Retrograde vesicle tethering activity was measured in a cell-free assay in which Golgi membranes isolated from HEK293 cells expressing the indicated shRNAs and CFP-tagged GalT are incubated with vesicles containing YFP-tagged GalT. Tethering activity is based on co-localization of Golgi and vesicles. The tethering activity of PAQR11-deficient Golgi was normalized to results obtained with Golgi from PAQR11-replete (shCTL-transfected) cells, which were set at 1 (n=5 samples per condition with the exception of shPAQR11 #4, which had n=4). (B) The scatter plot shows the average lumen diameters of spheres formed in Matrigel by 344SQ cells stably transfected with scrambled control shRNA (shCTL) or one of two distinct PAQR11 shRNAs (shPAQR11#1 or shPAQR11#3). Lumen diameters were measured at day 10. Each dot represents values from a single cell. (C) The scatter plot shows average lumen diameters of spheres formed by 344SQ\_shPAQR11 cells transfected with EGFP alone (shPAQR11\_EGFP), wild-type PAQR11 (shPAQR11\_EGFP-PAQR11), or PAQR11 mutants that lack N- ( $\Delta$ N) or C- ( $\Delta$ C) terminal domains. The average sphere lumen diameters were measured at day 10. Each dot represents values from a single cell. P values from two-tailed Student's t-test or ANOVA for comparisons between 2 groups or more than 2 groups, respectively. Results from single experiments were replicated (n  $\geq$  2 experiments).



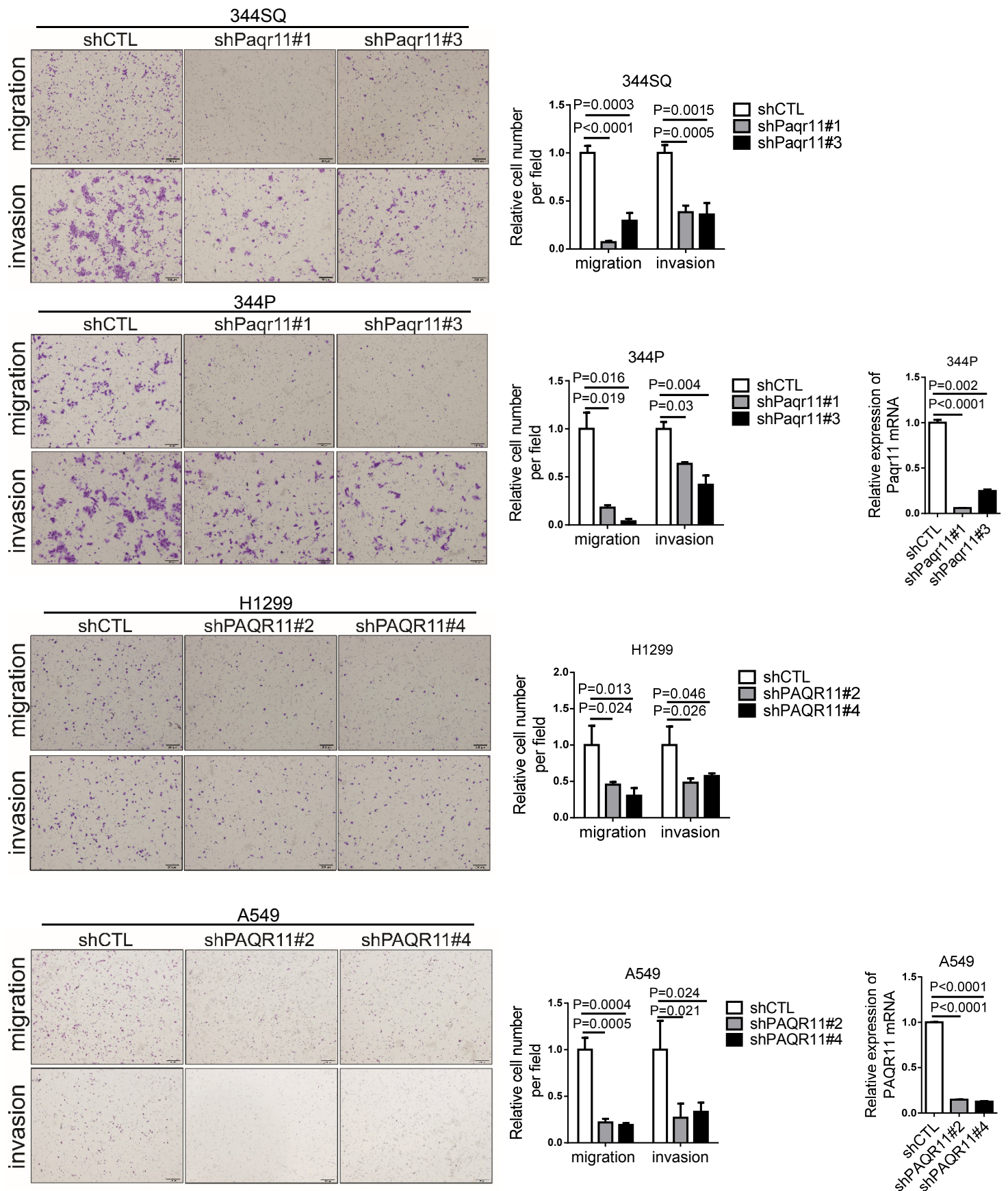
**Supplemental Figure 10. Protein-binding and Golgi localization functions of the N-terminus of PAQR11.** (A) Illustration of the predicted 7-transmembrane structure of PAQR11 (<https://www.predictprotein.org>). (B) Sodium dodecyl sulfate-polyacrylamide gel electrophoresis of proteins isolated by pull-down assays using 28 N-terminal amino acids (N-terminus) or 19 C-terminal amino acids (C-terminus) as bait. Collections of flow-through (lane 1) and subsequent washes with phosphate-buffered saline (PBS, lane 2), PBS + PBS with 0.1% Tween-20 (PBS-T, lane 3), PBS-T + 400 mM NaCl (lane 4), PBS-T + 800 mM NaCl (lane 5), and boiling (lane 6). Molecular weight markers (MW). To identify proteins that associated with the PAQR11 N-terminus, lane 4 of the gel was cut into pieces (1-10), and the proteins were eluted and subjected to liquid chromatography-tandem mass spectrometry (LC-MS/MS). (C) Confocal micrographs of 344SQ cells transiently transfected with constructs that express EGFP-tagged full-length PAQR11 or PAQR11 deletion mutants that lack amino acids 1-5 ( $\Delta$ N5), 1-10 ( $\Delta$ N10), 1-20 ( $\Delta$ N20), or 1-28 ( $\Delta$ N28). Cells were stained with anti-GM130 and counterstained with DAPI. EGFP and GM130 were merged with DAPI in pseudocolored images (far right column). Scale bars, 5  $\mu$ m. (D) Scatter plot shows the percentage of EGFP that co-localized with GM130 in each cell (dot). 344SQ\_shPAQR11 cells were stably transfected with EGFP alone (shPAQR11\_EGFP), EGFP-tagged full-length PAQR11 (shPAQR11\_EGFP-PAQR11), or EGFP-tagged  $\Delta$ N5 (shPAQR11\_EGFP-PAQR11 $\Delta$ N5). P values from two-tailed Student's t-test or ANOVA for comparisons between 2 groups or more than 2 groups, respectively. Findings in Supplemental Figures 10C and 10D were replicated ( $n \geq 2$  experiments).



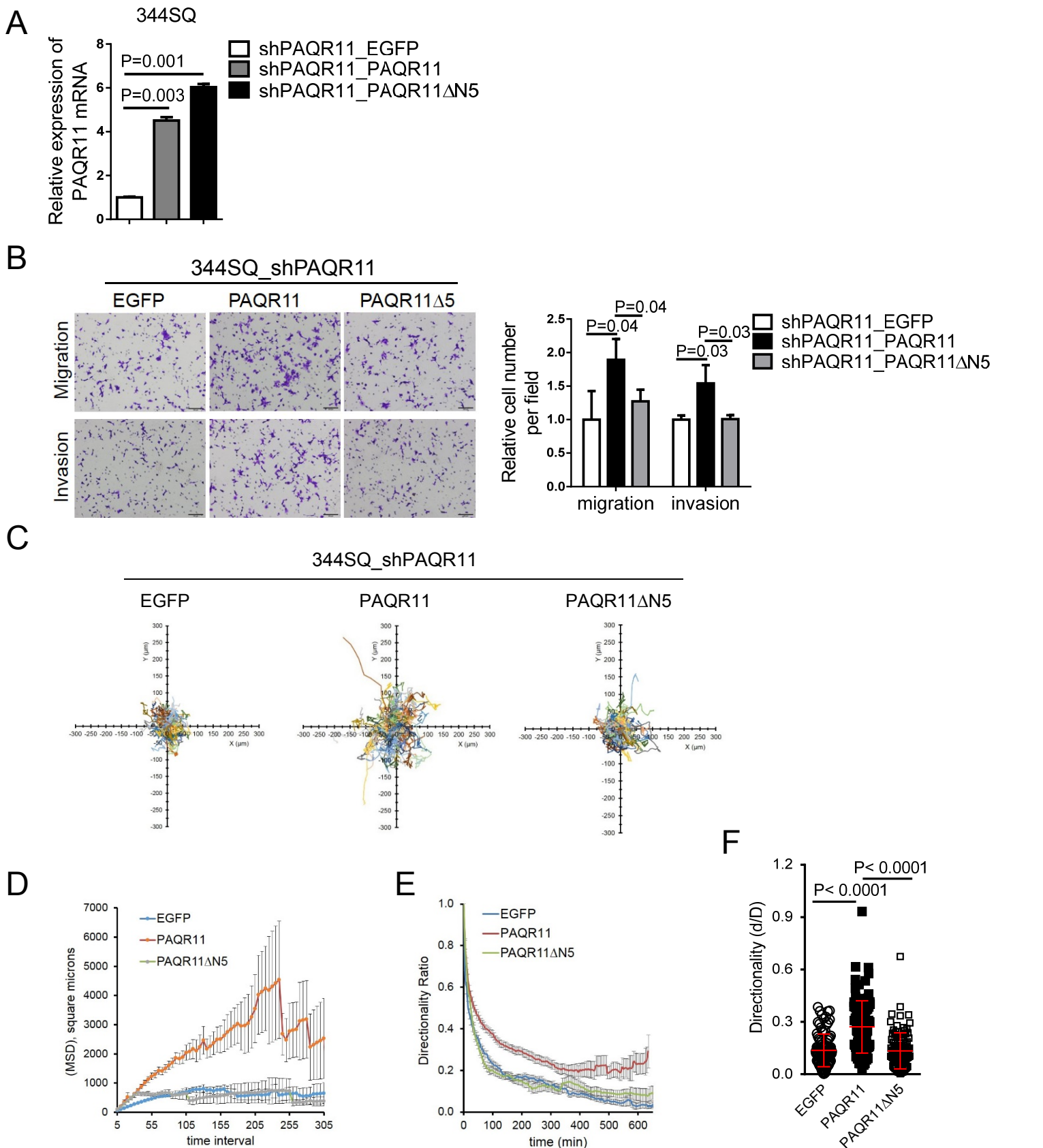
**Supplemental Figure 11. PAQR11 promotes lung adenocarcinoma metastasis.** (A) Bar graph shows the results of qPCR analysis of PAQR11 mRNA levels in flank tumors generated by subcutaneous injection of syngeneic, immunocompetent mice with 344SQ cells stably transfected with vectors expressing scrambled control shRNA (shCTL) or one of 2 distinct PAQR11 shRNAs (shPAQR11#1 or shPAQR11#3). Levels in 344SQ\_shCTL\_EGFP tumors were set at 1.0 (n=3 samples per condition). (B) Scatter plots show the numbers of metastases to mediastinal lymph nodes (left) and contralateral lung surfaces (right) visible at necropsy 4 weeks after injection of tumor cells. Each dot represents the results from a single mouse. Orthotopic lung tumors were generated in nude mice by intrathoracic injection with H1299 cells that had been stably transfected with scrambled control (shCTL) or one of 2 PAQR11 shRNAs (shPAQR11#2 or shPAQR11 #4). (C) Bar graph shows the results of qPCR analysis of PAQR11 mRNA levels in flank tumors generated by subcutaneous injection of syngeneic, immunocompetent mice with 393P cells stably transfected with vectors expressing PAQR11 or EGFP. Levels in 344SQ\_EGFP tumors were set at 1.0 (n=3 samples per condition). (D) Scatter plots of primary flank tumor weights (left) and lung metastasis numbers (right) per mouse necropsied 5 weeks after subcutaneous injection with 393P cells that do (PAQR11) or do not (EGFP) express ectopic PAQR11. Tumors were weighed, and metastases on lung surfaces were counted. Each dot represents the results from a single mouse. P values from two-tailed Student's t-test or ANOVA for comparisons between 2 groups or more than 2 groups, respectively.



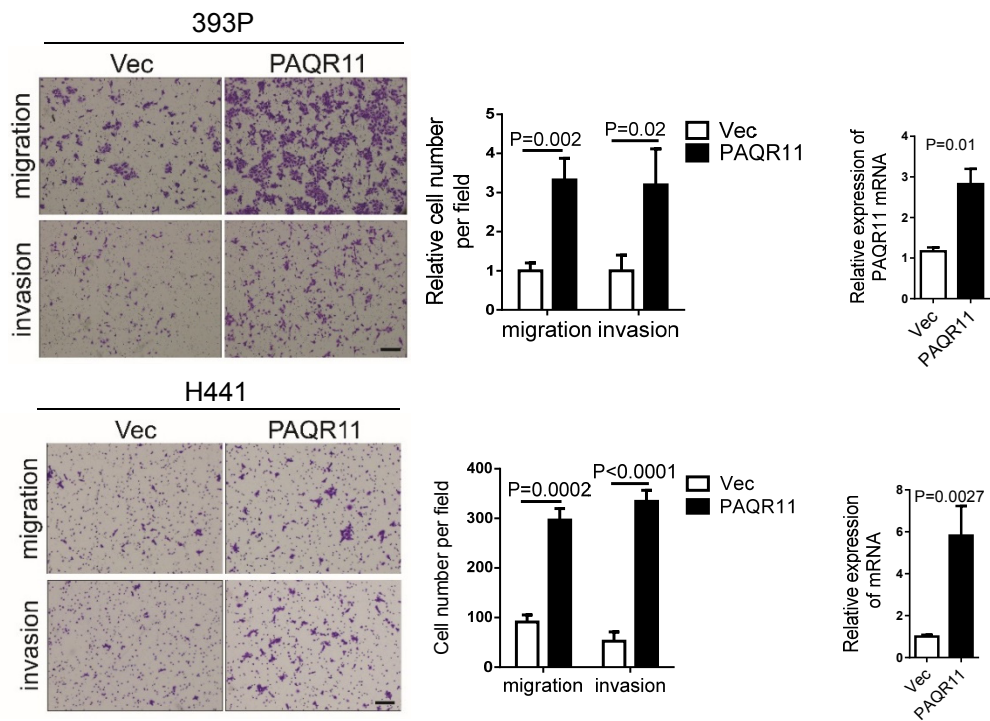
**Supplemental Figure 12. PAQR11 depletion reduces the migration and invasion of H1299 human lung cancer cells.** (A) Bright field micrographs of cells at the leading edges of scratch-wounded cultures of H1299 cells stably transfected with scrambled control shRNA (shCTL) or PAQR11 shRNA (shPAQR11). The bar graph shows the quantification of the percent wound closure 24 h and 36 h after placing the scratch wound (n=3 samples per condition). (B) Time-lapse tracing of movements of H1299 cells stably transfected with scrambled control shRNA (shCTL) or PAQR11 shRNA (shPAQR11). Movements of individual cells seeded at low density on plastic over 6 h indicated by colored lines. Bar graphs show the quantification of cell speed (left) and directionality (right) (n=3 samples per condition). (C) Bright field micrograph of a H1299 spheroid in collagen showing cells invading singly (red arrow). Scale bar, 100  $\mu\text{m}$ . The bar and whisker plot shows the quantification of single-cell invasions of H1299 cells stably transfected with scrambled control shRNA (shCTL) or PAQR11 shRNA (shPAQR11) (n=3 samples per condition). P values determined using two-tailed Student's t-test. Results from single experiments were replicated (n  $\geq$  2 experiments).



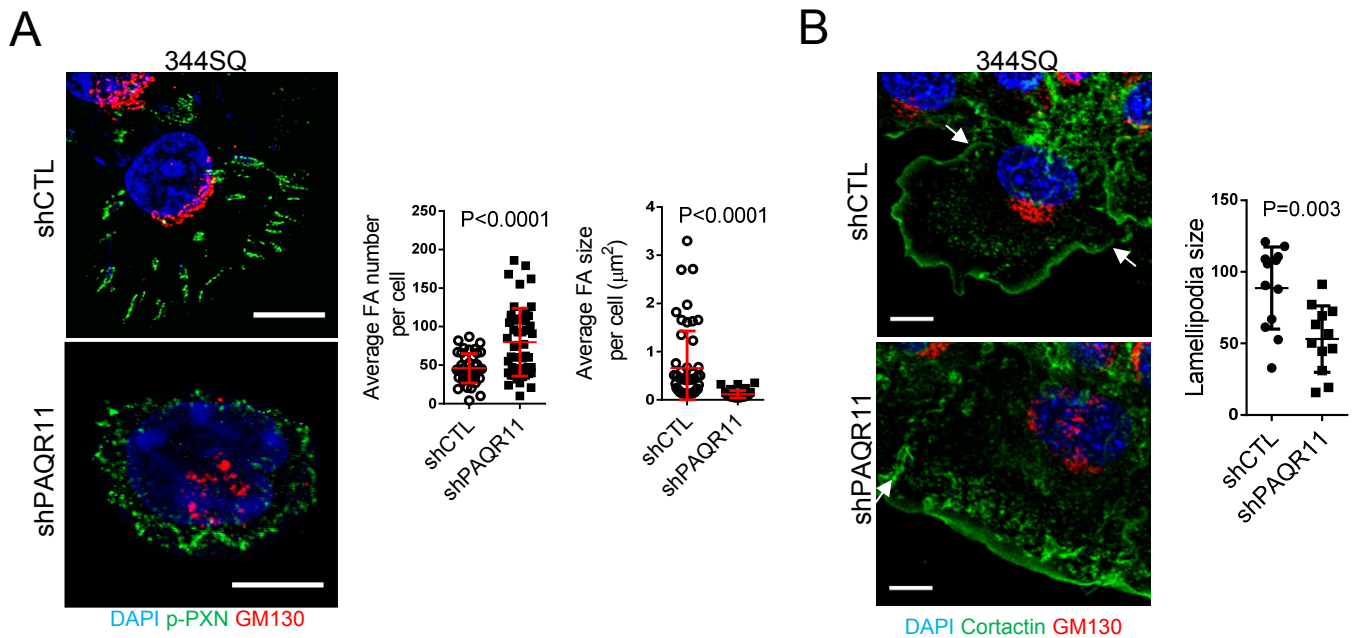
**Supplemental Figure 13. PAQR11 depletion reduces cell migratory and invasive activities.** Bright field micrographs of migrated and invaded murine KP cells (344SQ and 344P) and human lung cancer cells (H1299 and A549) in Boyden chambers. Cells were stably transfected with scrambled control shRNA (shCTL) or one of two distinct PAQR11 shRNAs. Migrated and invaded cells were stained with crystal violet (purple). Scale bars, 200  $\mu$ m. Bar graphs to the right of the images show the quantification of migrated and invaded cells (n=3 samples per condition). For 344P cells and A549 cells, the bar graphs to the far right show the results of qPCR analysis of PAQR11 mRNA levels in cells stably transfected with PAQR11 shRNAs or scrambled control shRNA expressed as a ratio (shPAQR11/shCTL). Levels in shCTL-transfected cells were set at 1.0 (n=3 samples per condition). P values from two-tailed Student's t-test or ANOVA for comparisons between 2 groups or more than 2 groups, respectively. Results from single experiments were replicated (n  $\geq$  2 experiments).



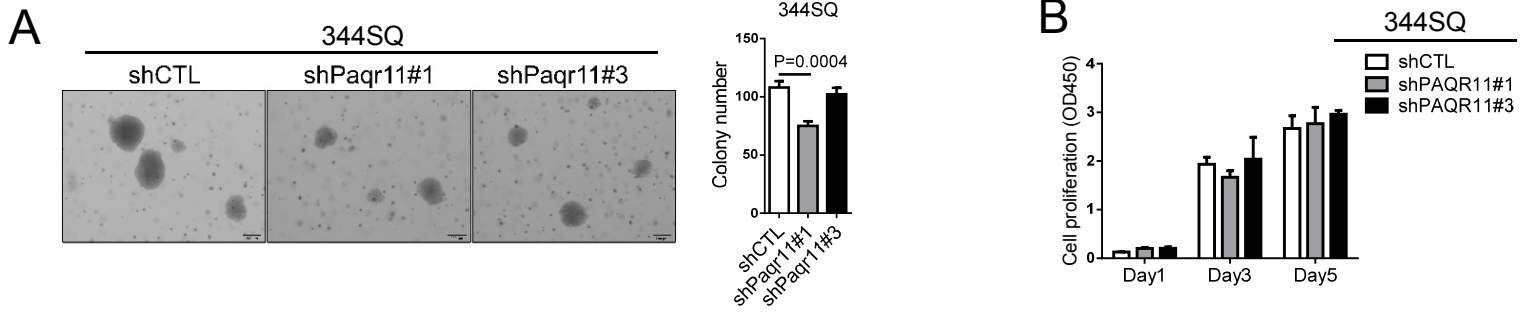
**Supplemental Figure 14. Loss of cell migration and invasion due to PAQR11 depletion are rescued by wild-type but not ΔN5 mutant PAQR11.** (A) Bar graph shows the results of qPCR analysis of PAQR11 mRNA levels in 344SQ\_shPAQR11 cells that have been stably transfected with vectors that express EGFP alone (shPAQR11\_EGFP), EGFP-tagged full-length PAQR11 (shPAQR11\_PAQR11), or EGFP-tagged ΔN5 mutant PAQR11 (shPAQR11\_PAQR11ΔN5). Levels in 344SQ\_shCTL\_EGFP cells were set at 1.0 (n=3 samples per condition). (B) Bright field micrographs of migrated and invaded cells in Boyden chambers stained with crystal violet. Scale bars, 200 μm. Bar graph shows the quantification of migrated and invaded cells (n=3 samples per condition). (C) Translated trajectories of 344SQ\_shPAQR11 cells stably expressing EGFP alone (EGFP) or EGFP-tagged full-length PAQR11 (PAQR11) or PAQR11ΔN5. (D-F) Mean squared displacements (D) and directionality ratio over time (E) or at the last point of trajectory (F) were measured in 344SQ\_shPAQR11 cells stably expressing EGFP or EGFP-tagged PAQR11 or PAQR11ΔN5 (n ≥ 100 cells per condition). P values from two-tailed Student's t-test or ANOVA for comparisons between 2 groups or more than 2 groups, respectively. Results from single experiments were replicated (n ≥ 2 experiments).



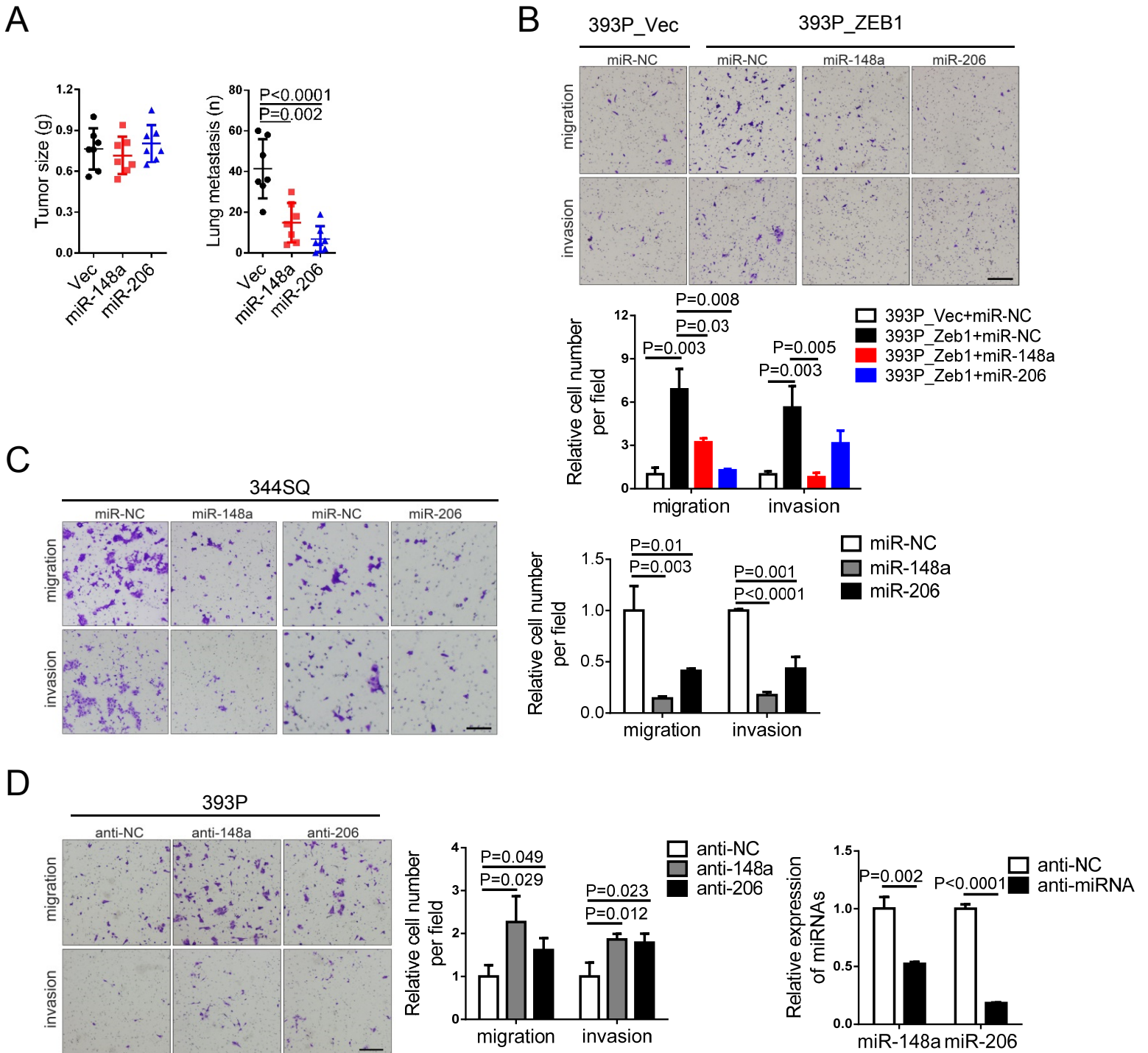
**Supplemental Figure 15. Ectopic PAQR11 expression increases cell migration and invasion.** Bright field micrographs of migrated and invaded cells in Boyden chambers stained with crystal violet (purple). 393P cells (top) and H441 cells (bottom) were stably transfected with vectors that express PAQR11 (PAQR11) or nothing (Vec). Scale bars, 200  $\mu$ m. Bar graphs adjacent to the micrographs show the quantification of migrated and invaded cells (n=3 samples per condition). Bar graphs to the far right show the results of qPCR assays of PAQR11 levels in cells stably transfected with PAQR11 or empty (Vec) expression vectors (n=3 samples per condition). P values determined using two-tailed Student's t-test. Results from single experiments were replicated (n  $\geq$  2 experiments).



**Supplemental Figure 16. PAQR11 enhances focal adhesion maturation and lamellipodia size.** (A) Confocal micrographs of Golgi (GM130, red), focal adhesions (phosphorylated paxillin [p-PXN], green), and nuclei (DAPI, blue) in 344SQ cells stably transfected with scrambled shRNA (shCTL, top) or PAQR11 shRNA (shPAQR11, bottom). Scale bars, 10  $\mu\text{m}$ . The scatter plots show the focal adhesion (FA) numbers (left) and areas (right) in each cell (dots). (B) Confocal micrographs of Golgi (GM130, red), lamellipodia (arrows delineate the edges of lamellipodial projections outlined by subcortical cortactin, green), and nuclei (DAPI, blue) in 344SQ cells stably transfected with scrambled shRNA (shCTL, top) or PAQR11 shRNA (shPAQR11, bottom). Scale bars, 10  $\mu\text{m}$ . Scatter plots show lamellipodia areas in each cell (dots). P values determined using two-tailed Student's t-test. Results from single experiments were replicated ( $n \geq 2$  experiments).



**Supplemental Figure 17. PAQR11 deficiency minimally inhibits anchorage-independent and –dependent tumor cell proliferation.** (A) Bright field micrographs of colonies in soft agar. The bar graph shows the quantification of the colonies (n=3 samples per condition). (B) The bar graph shows quantification of cell density in monolayer culture by WST-1 assays (n=3 samples per condition). P values from two-tailed Student's t-test or ANOVA for comparisons between 2 groups or more than 2 groups, respectively. Results from single experiments were replicated (n ≥ 2 experiments).



**Supplemental Figure 18. miR-148a and miR-206 suppress tumor cell metastatic properties.** (A) Scatter plots show the weights of subcutaneous tumors (left) and lung metastasis numbers (right) per mouse (dots). 344SQ cells that stably express ectopic miR-148a or miR-206 or empty vector (Vec) were subcutaneously injected into syngeneic, immunocompetent mice, which were necropsied after 6 weeks; the primary tumor was weighed, and metastases on lung surfaces were counted. (B, C) Bright field micrographs migrated and invaded 393P\_vector cells (B), 393P\_ZEB1 cells (B), and 344SQ cells (C) after transfection with miR-148a or miR-206 or control oligos (NC). Cells in Boyden chambers were stained with crystal violet (purple). Scale bars, 200  $\mu$ m. Bar graphs show the quantification of migrated and invaded cells that transiently express ectopic miRs (n=3 samples per condition). (D) Bright field micrographs of migrated and invaded 393P cells transfected with antagomiRs to miR-148a or miR-206 or control oligos (NC). Cells in Boyden chambers were stained with crystal violet (purple). Scale bars, 200  $\mu$ m. The bar graph to the right of the micrographs shows the quantification of migrated and invaded cells (n=3 samples per condition). The bar graph to the far right shows the results of qPCR assays of miR levels in cells transfected with antagomiRs or negative control (anti-NC). Levels in anti-NC-transfected cells were set at 1.0 (n=3 samples per condition). P values from two-tailed Student's t-test or ANOVA for comparisons between 2 groups or more than 2 groups, respectively. Results from single experiments were replicated (n  $\geq$  2 experiments).

## **SUPPLEMENTAL METHODS**

### **Reagents**

We purchased recombinant transforming growth factor beta (TGF $\beta$ ) from EMD-Calbiochem; microRNA (miRNA) mimics (miR-148a, miR-206, miR-200a, miR-200b, miR-200c, miR-182), SYBR Green, TRIzol, Lipofectamine 2000, fetal bovine serum (FBS), HEPES buffered media, Dulbecco's minimal essential medium (DMEM), RPMI Media 1640, Alexa Fluor-tagged secondary antibodies, Cell-Light Golgi-GFP, and DAPI from Life Technologies; puromycin from InvivoGene; paraformaldehyde from Electron Microscopy Sciences; Transwell and Matrigel-coated Boyden chambers from BD Biosciences; G418 from Corning; MDCK cells from ATCC; qScript cDNA superMix from Quanta Biosciences; the MinElute Reaction Cleanup kit from Qiagen; shRNAs against murine PAQR11 (TRCN0000326934 and TRCN0000326935), and shRNAs against human PAQR11 (TRCN0000062989 and TRCN0000062990) from Sigma; AffiGel from Bio-Rad; the Dual-Luciferase Reporter Assay System, pGL3-control reporter, and pRL-TK control reporter vector from Promega; DRAQ5 from Pierce Biotechnology; and Brefeldin-A from Cell Signaling Technology. We purchased primary antibodies against GM130 (#560066) from BD Transduction Laboratories; against PAQR11 (ab103749) and paxillin (ab2264) from Abcam; against golgin-97 (#13192), actin (#4970), acetylated  $\alpha$ -tubulin (D20G3), and vimentin (#5741) from Cell Signaling Technology; against phospho-paxillin (44-722G) and VSV-G (Clone: IE9F9) from Kerablast; against  $\alpha$ -tubulin (#T9026) from Sigma; and against ZEB1 (#sc-25388X) and GATA3 (#sc-9009) from Santa Cruz Biotechnologies. The EGFP-VSV-G (ts045) expression construct (Addgene plasmid #11912) was a gift from Dr. Jennifer Lippincott-Schwartz.

### **Cell Culture**

KP cells (307P, 344LN, 344P, 344SQ, 393LN, 393P, 412P, 531LN1, 531LN2, 531P1, 531P2, and 713P cells) were derived from KP mice as described previously (1). Human lung cancer

cells (H441, HCC827, H358, H226, H1819, A549, H157, Calu-1, and H1299 cells) were purchased (American Type Culture Collection). KP cell lines and human lung cancer cell lines were cultured in RPMI 1640 with 10% FBS. MCF-7 and MDA-MB-231 human breast cancer cell lines and MDCK cells were cultured in DMEM with 10% FBS. Cells were maintained at 37°C in an incubator with a humidified atmosphere containing 5% CO<sub>2</sub>. Cells were transfected with vectors using Lipofectamine 2000, and stable transfectants were selected for 2 weeks using puromycin (for the pLVX-puro vector) or G418 (for the pcDNA 3.1 and pEGFP-C3 vectors). Cell-Light BacMam baculoviral Golgi-RFP was used at 30 particles per cell. Where indicated, cells were treated with recombinant TGF- $\beta$  (5 ng/ml) for 3 days.

### **Vector construction**

Genomic DNA fragments containing miR-206 and miR-148a precursors were isolated by performing polymerase chain reaction (PCR) on 344SQ cells and then inserted into a pLVX-Puro expression vector (Clontech). The miR-200b/c/429 expression construct has been reported previously (1). The PAQR11 coding sequence was isolated by performing PCR on cDNA prepared from H1299 cells and then cloned into the pLVX-Puro vector. A C-terminal Flag tag was introduced by performing PCR. PAQR11 deletion mutants lacking 28 N-terminal amino acids or 18 C-terminal amino acids were created by PCR, and full-length or deletion mutants were inserted into the pEGFP-C3 vector (Clontech). Reporter plasmids containing miR-148a or miR-206 promoters were constructed by amplifying the upstream sequence of miR-148a (-2,000 to 0) and miR-206 (-2,000 to +190) from genomic DNA prepared from 344SQ cells and then subcloning the products into PGL3-Basic vector (Promega). Full-length murine and human PAQR11 3'-UTR sequences were isolated from genomic DNA prepared from 344SQ and H1299 cells, respectively, and cloned into the pCI-neo-hRL vector (2). Site-directed mutagenesis was carried out by performing PCR. The primer sequences for molecular cloning are listed in Supplementary Table S6.

### **Cell Proliferation and Colony Formation**

Cell proliferation assays were performed using Cell Proliferation Reagent WST-1 (Roche) according to the manufacturer's protocol. The soft agarose colony formation assays were performed as described previously (3).

### **Cell Migration and Invasion**

Multicellular spheroids in hanging drops (4) were generated by creating suspensions of 2000 cells in 25- $\mu$ l droplets for 48 h to ensure multicellular aggregation, at which point the spheroids were washed with medium, mixed with 2 mg/ml of rat-tail collagen I solution (SERVA Electrophoresis GmbH), and polymerized at 37°C in an incubator. Complete medium was supplied, and the spheroids were imaged under a bright-field microscope 12 or 24 h after seeding. Multi-cellular (collective) protrusions and single migratory cells were counted. As described previously (3), cell migration and invasion assays were performed in Transwell and Matrigel-coated Boyden chambers, respectively, and wound healing assays were performed on 80% confluent cells in monolayer subjected to scratch wounds. For single-cell tracing experiments, live cell microscopy was carried out for 6-12 hours on 0.5 mg/ml collagen I-coated microwell plates under a Nikon Eclipse Ti live cell imaging microscope (Nikon corporation, Tokyo, Japan) using Differential Interference Contrast imaging mode with a 20X / 0.75 NA dry objective. Centroids of individual cells were computed for tracking analysis with Imaris (Bitplane, Concord, MA). Cells were excluded from the analysis that migrated out of the field, underwent cell division or blebbing, or were non-motile as defined by movement of less than one cell diameter (~10  $\mu$ m). A total of 50-100 cells were analyzed per condition.

### **Quantitative RT-PCR**

Total RNA was isolated from cells using TRIzol and subjected to reverse transcription using the qScript cDNA superMix and quantitative PCR (qPCR) analysis with SYBR Green. mRNA levels were normalized on the basis of ribosomal protein L32 (Rpl32) mRNA. MicroRNA levels were quantified using stem-loop RT-PCR assays (5). The primer sequences for qPCR are listed in Supplementary Table S6.

### **Animal Husbandry**

All mouse studies were approved by the Institutional Animal Care and Use Committee at The University of Texas MD Anderson Cancer Center. Immunocompetent 129/Sv mice syngeneic to the KP cells were bred in-house and were injected subcutaneously in the right flank with tumor cells (n = 8-10 mice per group) and necropsied after 5 weeks; primary tumors were weighed, and lung metastases on the pleural surfaces were counted. Mice received standard care and were euthanized according to the standards set forth by the Institutional Animal Care and Use Committee.

### **Generation of Polarized Spheres**

As described previously (1), 344SQ cells were seeded over a layer of growth factor-reduced Matrigel (BD Biosciences) and cultured in RPMI 1640 with 10% FBS and 2% Matrigel, which was changed every 2–3 d. Spheres were imaged under phase-contrast microscopy after 8 d.

### **Promoter and 3'-UTR Activities**

For the promoter assays, cells were seeded on 48-well plates ( $5 \times 10^4$  cells/well) and transiently transfected 24 h later with 200 ng of luciferase reporter plasmids and 50 ng of pRL-TK control vector. For the 3'-UTR assays, 3'-UTR reporters (10 ng), pGL3-control (50 ng), and miRNA mimics (10 nM) were co-transfected into cells. After 24 h, luciferase activity was measured using the Dual-Luciferase Reporter Assay System (Promega).

## **Chromatin Immunoprecipitation**

As described previously (3), cell lysates were subjected to cross-linking followed by sonication with a Cole-Parmer GEX-130 ultrasonic processor using 50% power (pulse on for 10 s, pulse off for 10 s; 20 cycles) and immunoprecipitation with anti-ZEB1, anti-GATA3, or anti-rabbit IgG (Santa Cruz). DNA was eluted and purified using the MinElute Reaction Cleanup kit and subjected to PCR or quantitative PCR. PCR primers are listed in Supplementary Table S6.

## **Statistical Analysis**

Unless mentioned otherwise, the results shown are representative of replicated experiments and are the means  $\pm$  standard deviations from triplicate samples or randomly chosen cells within a field. Statistical evaluations were carried out with Prism 6 (GraphPad Software, Inc.). Unpaired 2-tailed Student t-tests were used to compare the mean values of 2 groups. ANOVA was used for analysis of parametric data. ANOVA with Dunnett's test was used for comparing multiple treatments to a control. ANOVA with a Bonferroni test was used when making multiple pair-wise comparisons between different groups. *P* values < 0.05 were considered statistically significant. The Kaplan–Meier method with log-rank test was used to evaluate overall survival curves for patients from a pan-cancer analysis (6) and from a previously compiled compendium of independent lung adenocarcinoma cohorts (7). The latter includes expression profiling datasets for 11 previously reported human lung adenocarcinoma cohorts (n = 1,492 tumors) (7), with the addition of another dataset from Sato et al. (8). Patients represented in both the Shedden and Chitale datasets (n=88 patients) were first removed from the Shedden dataset, and one patient from Bild dataset thought to potentially represent SQCC was also removed (leaving n = 1,586 tumors in total). For the pan-cancer analysis, we collected expression data on 9,105 tumors of various histological subtypes (ACC project, n=79; BLCA, n=342; BRCA,

n=1072; CESC, n=299; CHOL, n=34; COAD/READ, n=632; DLBC, n=27; GBM, n=157; HNSC, n=506; KICH, n=65; KIRC, n=526; KIRP, n=256; LAML, n=160; LGG, n=458; LIHC, n=353; LUAD, n=491; LUSC, n=480; MESO, n=71; OV, n=261; PAAD, n=163; PCPG, n=178; PRAD, n=436; SARC, n=243; SKCM, n=428; TGCT, n=121; THCA, n=498; THYM, n=111; UCEC, n=529; UCS, n=56; UVM, n=73), for which RNA-seq data (v2 platform) and survival data were available, from The Cancer Genome Atlas(6). Patient survival was capped at 15 years.

## Study Approval

Prior to conducting the animal studies reported herein, they were reviewed and approved by the Institutional Animal Care and Use Committee at The University of Texas MD Anderson Cancer Center (Houston, Texas).

1. Gibbons DL, Lin W, Creighton CJ, Rizvi ZH, Gregory PA, Goodall GJ, Thilaganathan N, Du L, Zhang Y, Pertsemlidis A, et al. Contextual extracellular cues promote tumor cell EMT and metastasis by regulating miR-200 family expression. *Genes & development*. 2009;23(18):2140-51.
2. Gregory PA, Bert AG, Paterson EL, Barry SC, Tsykin A, Farshid G, Vadas MA, Khew-Goodall Y, and Goodall GJ. The miR-200 family and miR-205 regulate epithelial to mesenchymal transition by targeting ZEB1 and SIP1. *Nat Cell Biol*. 2008;10(5):593-601.
3. Ahn YH, Gibbons DL, Chakravarti D, Creighton CJ, Rizvi ZH, Adams HP, Pertsemlidis A, Gregory PA, Wright JA, Goodall GJ, et al. ZEB1 drives prometastatic actin cytoskeletal remodeling by downregulating miR-34a expression. *The Journal of clinical investigation*. 2012;122(9):3170-83.
4. Foty R. A simple hanging drop cell culture protocol for generation of 3D spheroids. *Journal of visualized experiments : JoVE*. 2011(51).
5. Chen C, Ridzon DA, Broomer AJ, Zhou Z, Lee DH, Nguyen JT, Barbisin M, Xu NL, Mahuvakar VR, Andersen MR, et al. Real-time quantification of microRNAs by stem-loop RT-PCR. *Nucleic acids research*. 2005;33(20):e179.
6. Cancer Genome Atlas Research N, Weinstein JN, Collisson EA, Mills GB, Shaw KR, Ozenberger BA, Ellrott K, Shmulevich I, Sander C, and Stuart JM. The Cancer Genome Atlas Pan-Cancer analysis project. *Nature genetics*. 2013;45(10):1113-20.
7. Yang Y, Ahn YH, Chen Y, Tan X, Guo L, Gibbons DL, Ungewiss C, Peng DH, Liu X, Lin SH, et al. ZEB1 sensitizes lung adenocarcinoma to metastasis suppression by PI3K antagonism. *The Journal of clinical investigation*. 2014;124(6):2696-708.
8. Sato M, Larsen JE, Lee W, Sun H, Shames DS, Dalvi MP, Ramirez RD, Tang H, DiMaio JM, Gao B, et al. Human lung epithelial cells progressed to malignancy through specific oncogenic manipulations. *Mol Cancer Res*. 2013;11(6):638-50.



Supplemental Table 1. Golgi-associated genes upregulated by Zeb1

Gene Symbol	Fold change (Zeb1/Vec)	P value
Cnksr2	326.2987832	9.65E-05
Kif13a	30.61997783	4.93E-04
Rgs20	14.10207247	1.51E-03
Copz2	7.03458222	3.45E-04
Paqr11	6.983606232	3.87E-06
Sytl2	6.574838185	1.12E-04
Abca5	4.503068869	1.60E-04
Sec24b	4.007527067	6.66E-04
Cog1	3.69568258	1.94E-03
Manea	3.673839893	2.79E-04
Rab13	3.309775939	7.57E-05
Gga2	3.00028125	1.03E-04
Ap1m1	2.926032165	4.71E-04
Golim4	2.924456489	1.84E-05
Glg1	2.729698665	1.46E-03
Chst12	2.700505879	6.16E-03
Mapk3	2.683112597	2.89E-05
Ap3s1	2.527089714	3.38E-05
Yipf5	2.37751318	1.72E-03
Gkap1	2.367215358	1.49E-03
Tmed7	2.358155889	1.65E-04
Wipi1	2.30862254	4.71E-03
Rab38	2.298244743	3.86E-03
Chst11	2.224661828	9.35E-03
Acbd3	2.21800583	4.86E-03
Rab14	2.177932563	1.64E-04
Sh3glb1	2.13128696	1.14E-03
Ap1s2	2.129382915	2.75E-04
Dym	2.112362688	1.30E-03
Mapre1	2.097938575	4.86E-03
Rock1	2.09091141	9.66E-03
Slc35a2	2.044415766	6.19E-04
Vamp3	2.008775696	3.06E-05

Supplemental Table 2. PAQR11 binding partners.

<b>Gene Symbol*</b>	<b>Name*</b>	<b>Function in Golgi-Associated Trafficking<sup>#</sup></b>
<i>COPA</i>	Coatamer protein complex, subunit alpha	COPI-mediated retrograde vesicle transport
<i>COPB1</i>	Coatamer protein complex, subunit beta 1	COPI-mediated retrograde vesicle transport
<i>COPB2</i>	Coatamer protein complex, subunit beta 2 (beta prime)	COPI-mediated retrograde vesicle transport
<i>COPG1</i>	Coatamer protein complex, subunit gamma 1	COPI-mediated retrograde vesicle transport
<i>ANXA1</i>	Annexin A1	Positive regulation of vesicle fusion
<i>ANXA2</i>	Annexin A2	RAB GTPase binding; positive regulation of vesicle fusion
<i>ANXA5</i>	Annexin A5	Calcium and membrane phospholipid binding
<i>KIF2A</i>	Kinesin heavy chain member 2A	Motor activity; microtubule-based movement
<i>KIFC1</i>	Kinesin family member C1	Microtubule motor activity; microtubule-based movement
<i>KIF22</i>	Kinesin family member 22	Microtubule motor activity; microtubule-based movement
<i>SEC24A</i>	SEC24 homolog A, COPII coat complex component	Endoplasmic reticulum to Golgi vesicle mediated transport
<i>ARF1</i>	ADP-ribosylation factor 1	Post-Golgi vesicle-mediated transport; GTP binding; retrograde vesicle-mediated transport, Golgi to endoplasmic reticulum
<i>RAB11a</i>	RAB11A, member RAS oncogene family	Regulation of protein transport; vesicle-mediated transport
<i>NAT10</i>	N-acetyltransferase 10 (GCN5-related)	N-acetyltransferase activity
<i>DCTN1</i>	Dynactin 1	Microtubule-based transport; motor activity
<i>DCTN2</i>	Dynactin 2 (p50)	Microtubule-based transport; motor activity

\*Results from pull-down assay.

<sup>#</sup>Pooled from www.uniprot.org.

Supplemental Table 3. MicroRNAs correlated with ZEB1 and PAQR11 expression levels in KP cell lines

	<b>Correlation (vs. ZEB1)</b>	<b>Correlation (vs. PAQR11)</b>	<b>P value (E vs. M)</b>
<b>miR-200c</b>	R=-0.7343, P=0.0043	R=-0.6643, P=0.011	P<0.001
<b>miR-148a</b>	R=-0.7552, P=0.0031	R=-0.5594, P=0.031	P=0.017
<b>miR-206</b>	R=-0.7063, P=0.0065	R=-0.9371, P<0.001	P<0.001

Supplemental Table 5. PAQR11 levels are correlated with EMT status in human breast and lung cancer cohorts.

Gene	Breast Tumors (n=1,340)		Lung Adenocarcinomas (n=1,492)	
	T-Statistic	P Value	T-Statistic	P Value
<i>PAQR11</i>	11.866794	$5.91378 \times 10^{-31}$	16.5331756	$1.66279 \times 10^{-56}$
<i>SNAI1</i>	13.31414857	$4.50945 \times 10^{-38}$	20.01339049	$4.98597 \times 10^{-78}$
<i>SNAI2</i>	35.58069896	$1.0759 \times 10^{-195}$	33.21001237	$5.7945 \times 10^{-179}$
<i>TWIST1</i>	26.4564336	$2.0882 \times 10^{-124}$	32.59931258	$2.052 \times 10^{-176}$
<i>VIM</i>	36.27593397	$3.2081 \times 10^{-201}$	20.78884469	$1.72268 \times 10^{-84}$
<i>CDH2</i>	16.46178802	$1.3763 \times 10^{-55}$	16.56927569	$1.00197 \times 10^{-56}$
<i>CDH1</i>	-12.66037718	$8.86651 \times 10^{-35}$	-12.93549372	$3.05176 \times 10^{-36}$

Supplemental Table 6. Primer sequences.

qPCR primers		
Gene	Forward (5'-3')	Reverse (5'-3')
Paqr11 (mouse)	CACGATGGGATTTTCTCCAGCC	CAAACAGGTGCCAGATGGCATG
PAQR11(human)	TCTCCAGCCTTGGTGGTGACAT	ACAAACAGGTGCCAGATGGCGT
Rpl32(mouse)	GGAGAAGTTTCAAGGCCAG	TGCTCCATAAACCAGATGTTTG
RPL32 (human)	CCTTGTGAAGCCCAAGATCG	TGCCGGATGAACCTTCTGGT
Vim (mouse)	GCGTGGCTGCTTCAAGAC	ATGGCGTCGGCCAGCAGAA
Zeb1 (mouse)	GCTCAGCCAGGAACCCGACAG	TGGGCACCCTCTGCCACACA
Zeb2 (mouse)	AGCGCGAGAGAAGGGCAC	CCCGTTTCATCAGCAGCTCGG
Snai1 (mouse)	CCCAGGCCGTAGAGCTGA	GCTTTGCCACTGTCTCTCATC
Snai2 (mouse)	ATCCTCACCTCGGGAGCATA	TGCCGACGATGTCCATACAG
Cdh1 (mouse)	TACGGCGTGGTGAGGACGA	GCCACACGGGGAGACTTGC
Cdh2 (mouse)	CCTCCAGAGTTTACTGCCATGAC	CCACCACTGATTCTGTATGCCG
VIM (human)	GGAACAGCATGTCCAAATCGA	GCCGTGAGGTCAAGGCTTG
ZEB1 (human)	CACTGGTGGTGGCCATTAC	TGCACCATGCCCTGAGG
SNAI2 (human)	TGTGTGGACTACCGCTGCTC	GAGAGGCCATTGGGTAGCTG
CDH1 (human)	GACACACCCCTGTTGGTGT	CAGCCATCCTGTTTCTCTTTCAA
CDH2 (human)	ATCTCGGGTCAGCTGTCGG	GGCTATCTGCTCGCGATCC
Gata3	GTTCTCTCGACCCCTTCTAC	TTCATGATACTGCTCCTGCG
Mapre1	GAAACCTCTCGGCTCCAGTACT	CACACCAGGATCTTTTCGCACC
Abca5	GGCTCTCAATGTGGTGCGTTCT	TACTCCAGGTCTGGATGGCTTC
Copz2	GGATCTTCTCCGAGAATGAGC	ACCAAGAAGGCTCCGTCCATGT
Rab13	ATCCGAACCGTGGACATAGAGG	ATGGTCCACGGTAATAGGCGG
Rab14	GCAGATTTGGGATACAGCAGGG	GGTGAGATTCCTTGCCTGTGC
Rab38	TGTGACCAAGGGAAGGATGTGC	TGACCAGGCATCTTGGGCTTC
Golim4	GAGCATCTGGAGGAAGAACACG	TGTAGTGCCTTGGTCGAATGC
Sec24b	CCTTAGTGTGCTTTCAGACAGCC	ATGTTGGCGAGAAGGCAGACAG
Vamp3	AGACCAGAAGCTCTCGGAGCTA	ACCAGGACACTGATCCCTATCG
Kif13a	GACCAGTGTGAGTACAGTGG	CCAGGAACCTTCTGTGACAGTC
Yipf5	GAAGTGGAGGACCTACAGCAA	TGCCCAGTGTATGTCTGCTGTG
Tmed7	TGACAACGCCAAGCAGTGCTTC	CTTTACCATCAGGATCTTCCAATCG
Rgs20	TCAGAACAGACATTCAGCATGTG	GGCTGGAGTGACCATCAGGTTA
Gkap1	CTGACCTTGAGAAGGCGTTGCT	CTTGCCCTGGTGGTCTTCTCTT
Sh3glb1	CCAGCAACAACAGGAAGGCTAG	TTAGCCAGTCGGATCCATTCC
Wipi1	GAGTTCTGTGGAGCAGCTTGAC	GACGTTTATCTGCCGAGGTTTTG
Mapk3	GGCTTTCTGACGGAGTATGTGG	GTTGGAGAGCATCTCAGCCAGA
Ap1m1	CGCAGACCACTGACAGCAAGAT	TTCTGAACGCCAGGACACAGCA
Ap3s1	CGCAACAGCAAATCATCAGGGAG	TGAGCTTGTGTGACAGCCTCC
Ap1s2	GATGTGCAGCTTCTTGTAGTGG	TCCACGTAACGATGGATTATTTCC
Cog1	AGGAAGTCTGCTCCAACAGAG	CCTGAGAAGCAGTGTGAGTGTG
Glg1	AAGTGGTGCAGTGAGAAGACGG	CGGACTCTAAGTCCGTTGAGGTT
Gga2	TCATCAGGACCTGGCAGCCTTA	GCAGAAAGACTCTGGATTCCACC
Syl2	TGAGCAAGTCCGTGCCAGCATT	GTCATGCCAGAGGAGCTGCTAA
Dym	CCTTCTGGAAGAGTTGCTCTGC	ACCTCCTTGTGGAAGAGTTGGC
Cnksr2	GACAGTTCTGCTCTCCAGGATC	GAACCTGGTTGCCACCATATG

Manea	TAGTCCTCCAGACGACATTGGC	ATCAGGTGGGTACCAAGACAGG
Chst11	CCTTCGGTGTGGACATCTGCTG	TGTCACCTGGTCCCGTCTCATC
Chst12	AGGCTACGACTGGTCCACTCAT	GGATGTCGTCAAAGAGCGGTC
Slc35a2	CCTCCAGTATGTTGCCATCAGC	GCTGCGATTCAACATGAGCACAG
Paqr11	CACGATGGGATTTTCTCCAGCC	CAAACAGGTGCCAGATGGCATG
Rock1	CACGCCTAACTGACAAGCACCA	CAGGTCAACATCTAGCATGGAAC
<b>miRNA qPCR primers</b>		
U6-RT	GTCGTATCCAGTGCAGGGTCCGAGGTATTTCGACTGGATACGACAAAATATG	
miR-148a-RT	GTCGTATCCAGTGCAGGGTCCGAGGTATTTCGACTGGATACGACAAAAG	
miR-206-RT	GTCGTATCCAGTGCAGGGTCCGAGGTATTTCGACTGGATACGACCCACAC	
MIR-200c-RT	GTCGTATCCAGTGCAGGGTCCGAGGTATTTCGACTGGATACGACTCCATC	
<b>miRNA realtime PCR primers</b>	<b>Forward (5'-3')</b>	<b>Reverse (5'-3')</b>
U6	GCGCGTCGTGAAGCGTTC	GTGCAGGGTCCGAGGT
miR-148a	C CGCTCAGTGCACACACAGAAC	GTGCAGGGTCCGAGGT
miR-206	C CGCTGGAATGTAAGGAAGTG	GTGCAGGGTCCGAGGT
MiR-200c	GTAATACTGCCGGTAATGATGC	GTGCAGGGTCCGAGGT
<b>ChIP primers</b>	<b>Forward (5'-3')</b>	<b>Reverse (5'-3')</b>
ChIP-P200b-E	TCAGATGGAGGGCCTGTCT	GACCTGCAGTGGACTAGCTTG
ChIP-P148a-E1+2	TGGAGACCACGCTCTACCCAG	CCTTATGCAAAATAAACGACGAAG
ChIP-P148a--E3	GTTATTCTTCTTTGCCCTCACTGG	GAGACAAAGTTCTGTAGTGCACCTGA
ChIP-P206-1k	AATGGCTCAACAGCTGCC	CCAGATGAGCATTCCAACAC
CHIP-pre-206	TTCTGCGTGACAAGTGCCT	CCATCGGCCTTGAAGAAG
<b>Clone primers</b>		
<b>Primers for promoter cloning (PGL3-Basic)</b>		
P148a-2k	GGGGTACCTCTAGTCATGTGGCCTCTCATC	CCGCTCGAGGTCTCAAAGACCAAACTGGCT
E12-MT	GAGCCGGACTAGGAGCCATATGACCATATGGAGTGCCGCACCC	GGGTGCCGCACTCCATATGGTCATATGGCTCCTAGTCCGGCTC
E3-MT	GGATGGCAGGGAGCACATATGCAGGACGAACTTCCAG	CTGGAAGTTTCGTCATATGTGCTCCCTGCCATCC
P206-2k	GGGGTACC CCTTCAGCAAAATCTTGCTAGT	CCGCTCGAGGTAGAGGTAGATTTCCTGGGGAAGAG
P206-1k	GGAAGATCTCTATTTCTTACAGAGAATTTCTATGCC	CCCAAGCTTTGGGGAAGAGGGCACCTG
P206-500	GGGGTACCAGAGAAGGAGAAGGAGAAGAAGA	
P206+1	GGGGTACCCAGGCCACATGCTTCTT	
P206+50	GGGGTACCTGTAAGGAAGTGTGGTTTTGG	
P206+100	GGGGTACCCAGGAGAAATGCTGTTGAC	
P206-EMT	ACAGCTTCCCAGGCCGCTTCTTCTTTATATCCTCATAGATATCTCAGCA	TGCTGAGATATCTATGAGGATATAAAGAAGGAGCGCCCTGGGAAGCTGT
P206-GATA-MT1	GGCCACATGCTTTTATATCCTTACAGATATCTCAGCACTATGGAATGTAAGG	CCTTACATTCCATAGTCTGAGATATCTGTAAGGATATAAAGAAGCATGTGGCC
P206-GATA-MT2	GCCACATGCTTTTATATCCTCATAAAGATCTCAGCACTATGGAATGTAAGGA	TCCTTACATTCCATAGTCTGAGATCTTTATGAGGATATAAAGAAGCATGTGGC
<b>Primers for gene expression (pLVX-puro)</b>		
Paqr11 (mouse)	CCGCTCGAGATGCGGTTCAAGAAATCGATTCC	GCTCTAGAGTCATAAATGCCGAATAAAGTCTGTG
PAQR11 (human)	CCGCTCGAGATGCGGTTCAAGAAATCGATTCC	GCTCTAGAGTCATAAATGCCGATAAAGTC
MIR-148a	GTCACCTGAGCGTCCCATCTTAGGGGCTTTTC	GTCAGAATCACTAGATCTCAAACACTCAATCCCTG
MIR-206	CCGCTCGAGCATTTTCAAATCCACCTGCAAC	GGAATTCCTCTCAGAGCCAGTAGTTGTATAC
<b>Primers for gene expression (pEGFP-C3)</b>		
Paqr11 (mouse)	CCGCTCGAGATGCGGTTCAAGAAATCGATTCC	CGGGATCCCATAAATGCCGAATAAAGTCTGTGG
Paqr11 (mouse)-ΔN	CCGCTCGAGGCTGCCAATGCTACACACA	CGGGATCCCATAAATGCCGAATAAAGTCTGTGG
Paqr11 (mouse)-ΔC	CCGCTCGAGATGCGGTTCAAGAAATCGATTCC	CGGGATCCGTAGTGTACGGCAGCTGCC
PAQR11 (human)	CCGCTCGAGATGCGGTTCAAGAAATCGATTCC	CGGGATCCTCATAAATGCCGATAAAGTC

Paqr11 (human)-ΔN	CCGCTCGAGGCTGCTAACTGTTACACACAG	CGGGATCCTCATAAATGCCGCATAAAGTC
Paqr11 (human)-ΔC	CCGCTCGAGATGCGGTTCAAGAATCGATTC	CGGGATCCATGCACTGCAGCTGCC

**Movie 1. Golgi are more compact in mesenchymal 344SQ cells than epithelial 393P cells.** Time lapse live cell confocal microscopy of 344SQ cells (left) and 393P cells (right) transduced with Cell-Light BacMam Golgi-EGFP to mark Golgi (pseudocolored green). Nuclei were counterstained with DRAQ5 (pseudocolored red). Images were recorded at the interval of 2 minutes 30 seconds, for a period of 2 hour 30 minutes. Scale bar, 3  $\mu\text{m}$ . Movie compiled at 10 frames per second (fps).

**Movie 2. GalNAcT recovers more rapidly after photobleaching 344SQ cells than 393P cells.** Time lapse images in course of FRAP assay showing the Golgi apparatus in 344SQ and 393P cells transduced with Cell-Light BacMam Golgi-EGFP (intensity pseudocolored). Scale bar, 3  $\mu\text{m}$ . Arrowhead points to the bleached region. LUT bar shows intensity scale. Total run time: 1 min 58 sec. Movie compiled at 24 fps.

**Movie 3. Ectopic Zeb1 expression causes Golgi compaction in 393P cells.** 3D reconstruction of confocal Z-stacks of live 393P cells ectopically expressing empty vector or ZEB1. Cells were transduced with Cell-Light BacMam Golgi-RFP to mark Golgi (pseudocolored green). Nuclei was counterstained with DRAQ5 (pseudocolored magenta). Scale bar, 3  $\mu\text{m}$ . Movie compiled at 15 frames per second (fps).

**Movie 4. Ectopic ZEB1 expression in 393P cells accelerates GalNAcT recovery after photobleaching.** Time lapse images in course of FRAP assay showing the Golgi apparatus in 393P-Vector and 393P-ZEB1 cells transduced with Cell-Light BacMam Golgi-EGFP (intensity pseudocolored). Scale bar, 3  $\mu\text{m}$ . Arrowhead points to the bleached region. LUT bar shows intensity scale. Total run time: 5 min 42 sec. Movie compiled at 24 fps.

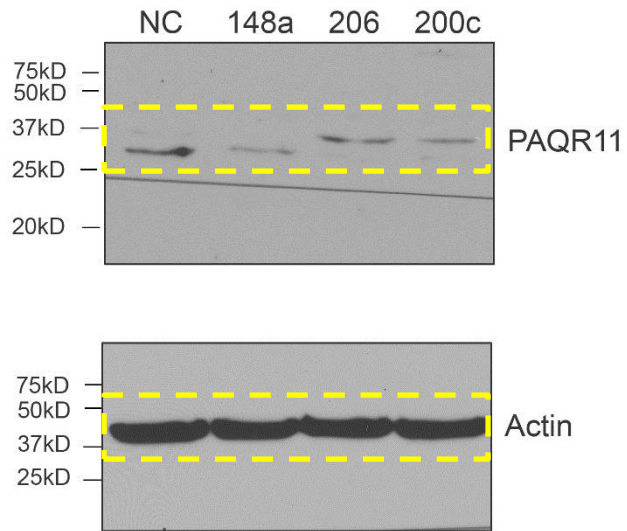
**Movie 5. PAQR11 is a Golgi resident protein.** Time lapse live cell confocal microscopy of 344SQ cells transduced with Cell-Light BacMam Golgi-RFP to mark Golgi (pseudocolored red), after transfection with PAQR11-EGFP (pseudocolored green). Nuclei were counterstained with DRAQ5 (pseudocolored blue). Images were recorded at the interval of 2 minutes for a period of 2 hour 40 minutes. Scale bar, 3  $\mu\text{m}$ . Movie compiled at 15 fps.

**Movie 6. PAQR11 depletion in 344SQ cells delays GalNAcT recovery after photobleaching.** Time lapse images in course of FRAP assay showing GalNAc recovery after photobleaching in 344SQ\_shCTL cells and 344SQ\_shPAQR11 cells transduced with Cell-Light BacMam Golgi-EGFP (intensity pseudocolored). Scale bar, 3  $\mu\text{m}$ . Arrowhead points to the bleached region. LUT bar shows intensity scale. Total run time: 6 min 2 sec. Movie compiled at 24 fps.

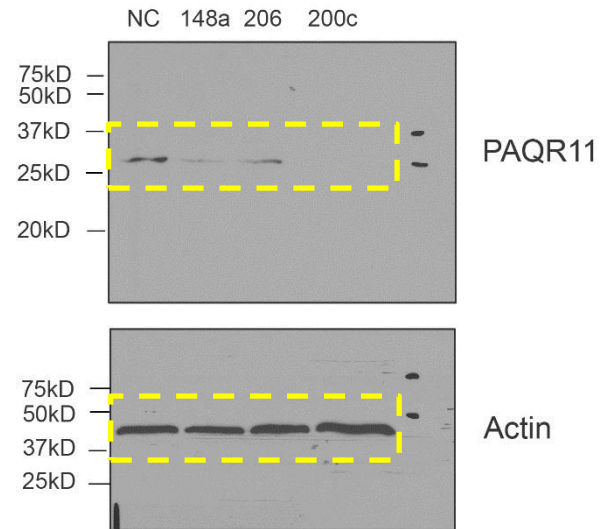
**Movie 7. Time lapse imaging showing that ectopic ZEB1 expression drives single cell migration in 393P spheroids seeded in 3-dimensional collagen.** Tumor cell spheroids of 393P\_Vec and 393P\_ZEB1 cells were embedded into collagen and imaged at intervals of 30 minutes for a period of 44 hours. Scale bar, 50  $\mu\text{m}$ . Movie compiled at 15 fps.

# Full unedited gel for Figure 6F

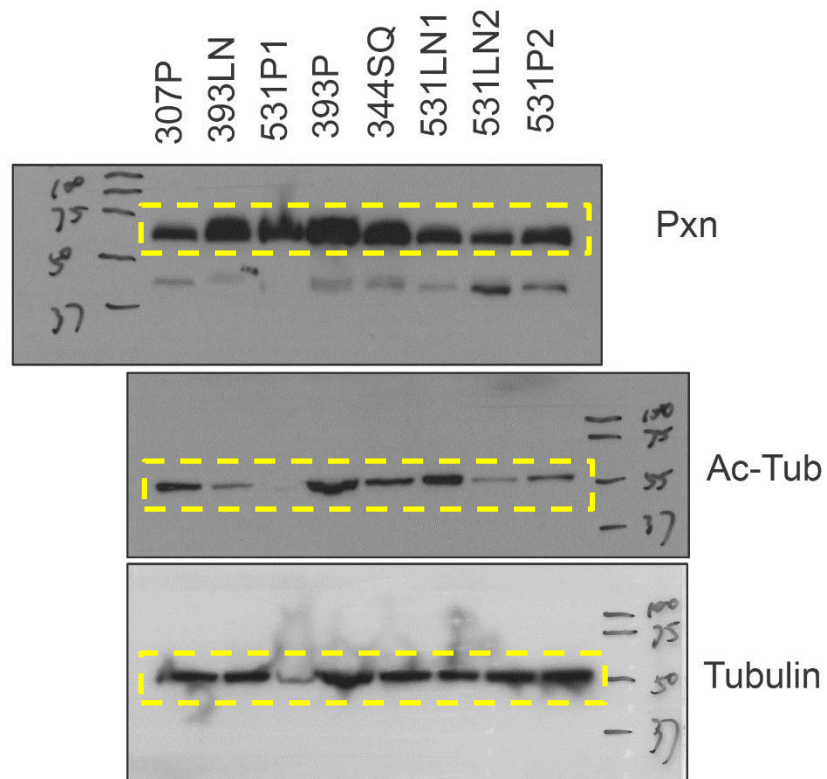
344SQ



H1299



# Full unedited gel for Figure S7B



# Full unedited gel for Figure S8A

